INSTITUT NATIONAL DE RECHERCHE EN INFORMATIQUE ET EN AUTOMATIQUE

Decoupled time-marching schemes in computational cardiac electrophysiology and ECG numerical simulation

Miguel A. Fernández — Nejib Zemzemi

N° 7022

August 2009

Thème BIO

ISSN 0249-6399 ISRN INRIA/RR--7022--FR+ENG

Decoupled time-marching schemes in computational cardiac electrophysiology and ECG numerical simulation

Miguel A. Fernández* , Nejib Zemzemi*†

Thème BIO — Systèmes biologiques
Projet REO

Rapport de recherche n° 7022 — August 2009 — 34 pages

Abstract: This work considers the approximation of the cardiac bidomain equations, either isolated or coupled with the torso, via first order semi-implicit time-marching schemes involving a fully decoupled computation of the unknown fields (ionic state, transmembrane potential, extracellular and torso potentials). For the isolated bidomain system, we show that the Gauss-Seidel and Jacobi like splittings do not compromise energy stability; they simply alter the energy norm. Time-step constraints are only due to the semi-implicit treatment of the non-linear reaction terms. Within the framework of the numerical simulation of electrocardiograms (ECG), these bidomain splittings are combined with an explicit Robin-Robin treatment of the heart-torso coupling conditions. We show that the resulting schemes allow a fully decoupled (energy) stable computation of the heart and torso fields, under an additional mild CFL like condition. Numerical simulations, based on anatomical heart and torso geometries, illustrate the stability and accuracy of the proposed schemes.

Key-words: Cardiac electrophysiology, forward problem, electrocardiogram, bidomain equations, heart-torso coupling, time discretization, explicit coupling, finite element method, Robin transmission conditions, stability analysis.

* INRIA, REO project-team
† Université Paris 11, Laboratoire de mathématiques d'Orsay, F–91405 Orsay Cedex, France

Unité de recherche INRIA Rocquencourt
Domaine de Voluceau, Rocquencourt, BP 105, 78153 Le Chesnay Cedex (France)
Téléphone : +33 1 39 63 55 11 — Télécopie : +33 1 39 63 53 30

Schémas de marche en temps découplés en éléctrophysiologie cardiaque computationnelle et simulation numérique de l'ECG

Résumé : Ce travail aborde l'appproximation des équations bidomaine, isolées ou couplées avec le thorax, par des schémas semi-implicites de premier ordre, permettant un calcul découplé des inconnues (état ionique, potentiel transmembranaire, potentiel extracellulaire et potentiel thoracique). Pour les équations bidomaine isolées, nous montrons que les découplages de type Gauss-Seidel et Jacobi ne compromettent pas la stabilité (au sens de l'énergie), ils simplement modifient la norme de l'énergie et les restrictions sur le pas de temps sont uniquement dues au traitement semi-implicite des termes de reaction nonlinéaires. Dans le cadre de la simulation numérique de l'électrocardiogramme (ECG), nous proposons de combiner ces techniques avec un traitement Robin-Robin explicite du couplage cœur-thorax. Les schémas ainsi obtenus permettent un calcul complètement découplé et stable (sous une simple condition CFL) des champs cardiaques et thoraciques. Des examples numériques, avec des géometries anatomiques de cœur et thorax, illustrent la stabilité et précision des schémas proposés.

Mots-clés : Électrophysiologie cardiaque, problème direct, électrocardiogramme, équation bidomaine, couplage cœur-thorax, discrétisation en temps, couplage explicite, méthode des éléments finis, conditions de Robin, analyse de stabilité.

1 Introduction

Computational models of cardiac electrophysiology typically incorporate the cell membrane activity and the intra- and extracellular components of cardiac tissue by means of the *bidomain model* (see e.g. [42, 38]). This mathematical model can be formulated as a *three-field* system (ionic state, transmembrane and extracellular potentials) coupling a non-linear reaction-diffusion equation, an elliptic equation and a non-linear system of ODE (alternative formulations are discussed in [24, 34]).

The rapid dynamics of the ODE system, acting on the reaction terms, lead to the presence of a sharp propagating wavefront, which often requires fine resolutions in space and in time. As a result, fully implicit time-marching is extremely difficult to perform since it involves the resolution of a large system of non-linear equations at each time step (see *e.g.* [24, 8, 33]). Attempts to reduce this computational complexity (without compromising too much numerical stability) consist in introducing some sort of explicit treatment within the time-marching procedure. For instance, by considering semi-implicit (see *e.g.* [43, 30, 14, 2, 5, 19]) or operator splitting (see *e.g.* [26, 44, 48]) schemes. All these approaches uncouple the ODE system (ionic state and non-linear reaction terms) from the electrodiffusive components (transmembrane and extracellular potentials). However, only a few works [43, 30, 2, 48] propose a decoupled (*Gauss-Seidel* like) time-marching of the three fields.

In this paper we go further in the investigation of this kind of decoupling techniques, by providing a general energy based stability analysis that covers both the Gauss-Seidel and the Jacobi like approaches. In particular, we show that these electrodiffusive splittings do not compromise the stability of the resulting scheme. They simply alter the energy norm and time step restrictions are uniquely dictated by the semi-implicit treatment of the ODE system and the non-linear reaction terms.

In the second part, we propose to extend these time-marching techniques to the numerical simulation of the electrocardiogram (ECG), namely, the *forward problem* of cardiac electrophysiolgy (see *e.g.* [29]). The bidomain equations have then to be coupled to a generalized Laplace equation, describing the electrical potential within the surrounding torso tissue. The heart-torso coupling is enforced through standard interface conditions, ensuring a perfect electrical balance (see *e.g.* [27, 38, 42]). This results in a coupled *four-field* problem (ionic state, transmembrane, extracellular and torso potentials) coupling a non-linear system of ODEs, a non-linear reaction-diffusion equation and two elliptic equations (see *e.g.* [29, 42]).

Traditionally, the heart-torso coupling has been treated using two different approaches (see *e.g.* [29]). The so called *heart-torso uncoupling* approximation (see *e.g.* [35, 37, 29, 4]) uncouples the heart and torso problems by neglecting the torso-to-heart electrical feedback (*i.e.* the heart is isolated). Although this approach is very appealing in terms of computational cost, it can compromise the accuracy of the corresponding ECG signals (see *e.g.* [29, 38, 4]). The second approach, the so called *heart-torso full coupling*, treats the heart-torso interface conditions in a fully implicit fashion and, therefore, requires the resolution of a large heart-torso system at each time step (see *e.g.* [43, 30, 38, 4]). To the best of our knowledge, none of the current approaches is able to provide accurate ECG

signals (*i.e.* close to heart-torso full coupling) with a decoupled computation of the extracellular and torso potentials.

In this paper, we introduce a series of time-marching schemes for ECG numerical simulation involving a fully decoupled computation of the ionic state, the transmembrane potential, the extracellular potential and the torso potential. The main idea consists in combining the above mentioned Gauss-Seidel or Jacobi like bidomain spplitings, with an explicit Robin-Robin treatment (derived from [1]) of the heart-torso coupling. An energy based stability analysis shows that the proposed schemes are stable under and additional mild CFL like condition. Note that, since the time discretization of the two (quasi-static) elliptic equations does not produce numerical dissipation, conventional explicit Dirichlet-Neumann heart-torso coupling might lead to numerical instability.

The remainder of this paper is organized as follows. In the next section we briefly recall the coupled system of equations describing the electrical activity of the heart and its interaction with the surrounding torso tissue. The time discretization of the bidomain equations is addressed in section §3, using Gauss-Seidel and Jacobi like eletrodiffusive splittings. The stability of the resulting schemes is analyzed by means of energy arguments. Section §4 is devoted to the discretization of the heart-torso system. The schemes analyzed in section §3 are then combined with a specific explicit Robin-Robin treatment of the heart-torso coupling. The energy based stability of the resulting schemes is investigated. Numerical evidence is provided in section §5, using realistic heart and torso geometries. A summary of the results and some concluding remarks are given in section §6.

2 Mathematical models

This section contains standard material (see *e.g.* [42, Chapter 2]). We introduce the notation and the coupled system of equations commonly used to model the electrical activity of the heart and its interaction with surrounding tissue (extramyocardial regions).

2.1 Isolated heart

The bidomain equations, originally derived in [46], are the most widely accepted mathematical model of the macroscopic electrical activity of the heart (see *e.g.* the monographs [42, 38]). This model is usually formulated in terms of three variables: the transmembrane potential $V_{\rm m}$, the extracellular potential $u_{\rm e}$ and the ionic state w (possibly vector valued). These space and time dependent variables are defined in $\Omega_{\rm H} \times (0,T)$, where $\Omega_{\rm H}$ and $(0,T)$ denote, respectively, the heart domain and the time interval of interest.

The governing equations consist of a coupled system of ODE, a nonlinear reaction-diffusion equation and an elliptic equation, with appropriate boundary

and initial conditions (see *e.g.* [42, 38]):

$$\partial_t w + g(V_{\rm m}, w) = 0, \quad \text{in} \quad \Omega_{\rm H} \times (0,T), \tag{2.1}$$

$$\chi_{\rm m}\partial_t V_{\rm m} + I_{\rm ion}(V_{\rm m}, w) - \mathrm{div}(\boldsymbol{\sigma}_{\rm i}\boldsymbol{\nabla} V_{\rm m}) - \mathrm{div}(\boldsymbol{\sigma}_{\rm i}\boldsymbol{\nabla} u_{\rm e}) = I_{\rm app}, \quad \text{in} \quad \Omega_{\rm H} \times (0,T), \tag{2.2}$$

$$-\mathrm{div}((\boldsymbol{\sigma}_{\rm i} + \boldsymbol{\sigma}_{\rm e})\boldsymbol{\nabla} u_{\rm e}) - \mathrm{div}(\boldsymbol{\sigma}_{\rm i}\boldsymbol{\nabla} V_{\rm m}) = 0, \quad \text{in} \quad \Omega_{\rm H} \times (0,T), \tag{2.3}$$

$$\boldsymbol{\sigma}_{\rm i}\boldsymbol{\nabla} V_{\rm m}\cdot\boldsymbol{n} + \boldsymbol{\sigma}_{\rm i}\boldsymbol{\nabla} u_{\rm e}\cdot\boldsymbol{n} = 0, \quad \text{on} \quad \Sigma \times (0,T), \tag{2.4}$$

$$\boldsymbol{\sigma}_{\rm e}\boldsymbol{\nabla} u_{\rm e}\cdot\boldsymbol{n} = 0, \quad \text{on} \quad \Sigma \times (0,T), \tag{2.5}$$

$$V_{\rm m}(\boldsymbol{x},0) = V_{\rm m}^0(\boldsymbol{x}), \quad w(\boldsymbol{x},0) = w^0(\boldsymbol{x}), \quad \forall \boldsymbol{x} \in \Omega_{\rm H}. \tag{2.6}$$

Here, $\chi_{\rm m} \stackrel{\rm def}{=} A_{\rm m}C_{\rm m}$ where $A_{\rm m}$ is a geometrical quantity, $C_{\rm m}$ denotes the membrane capacitance and tensors $\boldsymbol{\sigma}_{\rm i}$ and $\boldsymbol{\sigma}_{\rm e}$ represent, respectively, the intra- and extracellular conductivities. The term $I_{\rm ion}(V_{\rm m}, w) \stackrel{\rm def}{=} A_{\rm m} i_{\rm ion}(V_{\rm m}, w)$ denotes the ionic current across the membrane and $I_{\rm app}$ a given external current stimulus. The explicit expression of functions g and $i_{\rm ion}$ depends on the considered cell ionic model (see e.g. [42, 38] and the references therein). At last, $\boldsymbol{n}$ stands for the outward unit normal to $\Sigma \stackrel{\rm def}{=} \partial\Omega_{\rm H}$ (see Figure 1), and $V_{\rm m}^0$, w^0 are given initial data.

The boundary conditions (2.4)-(2.5) state that the intra- and extracellular currents do not propagate outside the heart. While (2.4) is a widely accepted condition (see *e.g.* [46, 27, 38, 42]), the enforcement of (2.5) is only justified under an isolated heart assumption (see [42, 38]). The coupled system of equations (2.1)-(2.6) is often known in the literature as *isolated bidomain* model (see *e.g.* [14, 15, 42]). The interested reader is referred to [16, 3, 7, 47] for the mathematical analysis of problem (2.1)-(2.6).

The choice of the formulation (2.1)-(2.6) is motivated by the decoupling time-marching schemes introduced in section §3. Other formulations of the bidomain equations and their impact on the performance of the algebraic solvers have been discussed in [24, 34]. A recent review of numerical methods for the bidomain equations can be found in [31].

Remark 2.1 *The complexity of* (2.1)-(2.6) *can be reduced by using, instead of* (2.2) *and* (2.4)*, the so-called monodomain approximation:*

$$\begin{aligned} \chi_{\rm m}\partial_t V_{\rm m} + I_{\rm ion}(V_{\rm m}, w) - \mathrm{div}\left(\boldsymbol{\sigma}\boldsymbol{\nabla} V_{\rm m}\right) &= I_{\rm app}, \quad \textit{in} \quad \Omega_{\rm H}, \\ \boldsymbol{\sigma}\boldsymbol{\nabla} V_{\rm m}\cdot\boldsymbol{n} &= 0, \quad \textit{on} \quad \Sigma, \end{aligned} \tag{2.7}$$

where $\boldsymbol{\sigma} \stackrel{\rm def}{=} \boldsymbol{\sigma}_{\rm i}(\boldsymbol{\sigma}_{\rm i} + \boldsymbol{\sigma}_{\rm e})^{-1}\boldsymbol{\sigma}_{\rm e}$ *is the bulk conductivity tensor (see e.g. [28, 13, 15, 36]). Note that* (2.7) *decouples de computation of* $V_{\rm m}$ *from that of* $u_{\rm e}$*. Under the isolating condition* (2.5)*,* (2.7) *can be interpreted as the zeroth-order approximation of* (2.2) *and* (2.4) *with respect to a parameter,* $0 \le \epsilon < 1$*, which measures the gap between the anisotropy ratios of the intra- and extracellular domains (see [13, 15] for details). Although several simulation analysis (see*

e.g. [13, 36]) suggest that the monodomain approximation may be adequate for some propagation studies in isolated hearts, it cannot be applied in all situations since it neglects the extracellular feedback into $V_{\rm m}$ (see e.g. [17, 13, 36] and Remark 2.3 below).

2.2 Coupling with torso: ECG modeling

The myocardium is surrounded by a volume conductor, $\Omega_{\rm T}$, which contains all the extramyocardial regions (see Figure 1). As a matter of fact, ECG signals monitor the electrical activity of the heart from potential measurements at the torso skin surface $\Gamma_{\rm ext}$. The torso volume is commonly modeled as a passive conductor (generalized Laplace equation), electrically coupled to the heart across the heart-torso interface Σ. The resulting coupled system can be formulated in

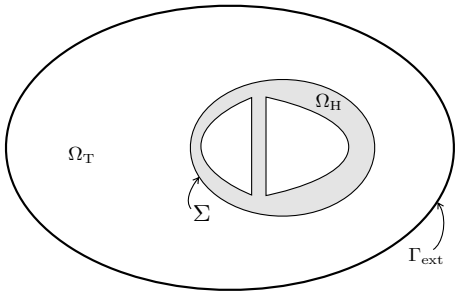

Figure 1: Two-dimensional geometrical description: heart domain $\Omega_{\rm H}$, torso domain $\Omega_{\rm T}$ (extramyocardial regions), heart-torso interface Σ and torso external boundary $\Gamma_{\rm ext}$.

terms of $V_{\rm m}$, $u_{\rm e}$, w and the torso potential $u_{\rm T}$, as follows (see *e.g.* [42, 38]):

$$\partial_t w + g(V_{\rm m}, w) = 0, \quad \text{in} \quad \Omega_{\rm H} \times (0,T), \tag{2.8}$$

$$\chi_{\rm m}\partial_t V_{\rm m} + I_{\rm ion}(V_{\rm m}, w) - \mathrm{div}(\boldsymbol{\sigma}_{\rm i}\boldsymbol{\nabla} V_{\rm m}) - \mathrm{div}(\boldsymbol{\sigma}_{\rm i}\boldsymbol{\nabla} u_{\rm e}) = I_{\rm app}, \quad \text{in} \quad \Omega_{\rm H} \times (0,T), \tag{2.9}$$

$$-\mathrm{div}((\boldsymbol{\sigma}_{\rm i} + \boldsymbol{\sigma}_{\rm e})\boldsymbol{\nabla} u_{\rm e}) - \mathrm{div}(\boldsymbol{\sigma}_{\rm i}\boldsymbol{\nabla} V_{\rm m}) = 0, \quad \text{in} \quad \Omega_{\rm H} \times (0,T), \tag{2.10}$$

$$-\mathrm{div}(\boldsymbol{\sigma}_{\rm T}\boldsymbol{\nabla} u_{\rm T}) = 0, \quad \text{in} \quad \Omega_{\rm T} \times (0,T), \tag{2.11}$$

$$\boldsymbol{\sigma}_{\rm T}\boldsymbol{\nabla} u_{\rm T} \cdot \boldsymbol{n}_{\rm T} = 0, \quad \text{on} \quad \Gamma_{\rm ext} \times (0,T), \tag{2.12}$$

$$\boldsymbol{\sigma}_{\rm i}\boldsymbol{\nabla} V_{\rm m} \cdot \boldsymbol{n} + \boldsymbol{\sigma}_{\rm i}\boldsymbol{\nabla} u_{\rm e} \cdot \boldsymbol{n} = 0, \quad \text{on} \quad \Sigma \times (0,T), \tag{2.13}$$

$$u_{\rm T} = u_{\rm e}, \quad \text{on} \quad \Sigma \times (0,T), \tag{2.14}$$

$$\boldsymbol{\sigma}_{\rm e}\boldsymbol{\nabla} u_{\rm e} \cdot \boldsymbol{n} = -\boldsymbol{\sigma}_{\rm T}\boldsymbol{\nabla} u_{\rm T} \cdot \boldsymbol{n}_{\rm T}, \quad \text{on} \quad \Sigma \times (0,T), \tag{2.15}$$

$$V_{\rm m}(\boldsymbol{x},0) = V_{\rm m}^0(\boldsymbol{x}), \quad w(\boldsymbol{x},0) = w^0(\boldsymbol{x}), \quad \forall \boldsymbol{x} \in \Omega_{\rm H}. \tag{2.16}$$

Here, $\boldsymbol{\sigma}_{\rm T}$ stands for the conductivity tensor of the torso tissue and $\boldsymbol{n}_{\rm T}$ for the outward unit normal to the external boundary $\Gamma_{\rm ext} \stackrel{\rm def}{=} \partial\Omega_{\rm T} \setminus \Sigma$ (see Figure 1).

The boundary condition (2.12) states that no current can flow from the external torso surface $\Gamma_{\rm ext}$, whereas (2.14)-(2.15) enforce a perfect electric balance between the heart and torso domains (see *e.g.* [46, 27, 38, 42]).

The coupled system of equations (2.8)-(2.16) is often known in the literature as *full bidomain* or *coupled bidomain* model (see *e.g.* [13, 42]). It can be considered as the state-of-the-art in the modeling of the ECG or, equivalently, the forward problem of cardiac electrophysiology (see *e.g.* [29, 38, 42]). The interested reader is referred to [6] for the mathematical analysis of problem (2.8)-(2.16), and to [29] (see also [4]) for a review of the numerical methods.

Remark 2.2 *A common approach to reduce the computational complexity of* (2.8)-(2.16) *consists in* uncoupling *the computation of* $(w, V_{\rm m}, u_{\rm e})$ *and* $u_{\rm T}$*, by neglecting the electrical torso-to-heart feedback (see* e.g. *[13, 35, 29]). Thus, the coupling condition* (2.15) *is replaced by*

$$\boldsymbol{\sigma}_{\rm e}\boldsymbol{\nabla} u_{\rm e} \cdot \boldsymbol{n} = 0, \quad \textit{on} \quad \Sigma, \tag{2.17}$$

which amounts to work with an isolated bidomain model, as described in the previous subsection. Thereafter, the torso potential $u_{\rm T}$ *is recovered by solving* (2.11) *with boundary conditions* (2.12)-(2.14)*. Despite this approach is very appealing in terms of computational cost, numerical evidence has shown that it can compromise the accuracy of the ECG signals (see e.g. [29, 38, 4] and the numerical study of subsection §5.3). The heart-torso uncoupling approximation is often further simplified by replacing the interface condition* (2.14) *by a (multi-) dipole representation of the cardiac source (see e.g. [22, 25]).*

Remark 2.3 *The monodomain approximation* (2.7) *can be combined with the heart-torso uncoupling framework of Remark 2.2 (see e.g. [25, 35, 4]). This yields a simplified mathematical model which allows a fully decoupled computation of* $V_{\rm m}$, $u_{\rm e}$ *and* $u_{\rm T}$. *However, as noticed in [4, Section 5.2] (see also [13]), without the uncoupling assumption* (2.17) *the monodomain approximation becomes*

$$\begin{aligned} \chi_{\rm m}\partial_t V_{\rm m} + I_{\rm ion}(V_{\rm m},w) - {\rm div}\left(\boldsymbol{\sigma}\boldsymbol{\nabla} V_{\rm m}\right) = I_{\rm app}, \quad & in \quad \Omega_{\rm H}, \\ \boldsymbol{\sigma}\boldsymbol{\nabla} V_{\rm m}\cdot\boldsymbol{n} = -\mu\boldsymbol{\sigma}_{\rm e}\boldsymbol{\nabla} u_{\rm e}\cdot\boldsymbol{n}, \quad & on \quad \Sigma, \end{aligned} \tag{2.18}$$

where $0<\mu<1$ *is a dimensionless parameter related to the local conductivities. Note that in* (2.18) $V_{\rm m}$ *and* $u_{\rm e}$ *are still coupled. Therefore, under the full heart-torso coupling* (2.14)-(2.15)*, the monodomain approximation does not reduce the computational complexity with respect to* (2.8)-(2.16).

3 Decoupled time-marching for the bidomain equation

In this section we analyze some time-discretization schemes for the isolated bidomain system (2.1)-(2.6). The main feature of the analyzed schemes is that they all allow a decoupled (Gauss-Seidel or Jacobi like) computation of $V_{\rm m}$ and $u_{\rm e}$, without compromising stability.

3.1 Preliminaries

In what follows, we will consider the usual Lebesgue and Sobolev spaces, $L^m(\Omega)$ and $H^m(\Omega)$ respectively ($m>0$), for a domain $\Omega\subset\mathbb{R}^3$. Then, for a given $X\subset\partial\Omega$ (with ${\rm meas}(X)>0$), we define $H^1_X(\Omega)$ as the subspace of $H^1(\Omega)$ with vanishing trace on X. The $L^2(\Omega)$-norm is denoted by $\|\cdot\|_{0,\Omega}$ and the vanishing mean value subspace of $L^2(\Omega)$ by $L^2_0(\Omega)$.

Problem (2.1)-(2.6) can be cast into weak form as follows (see *e.g.* [6]): for $t>0$, find $w(\cdot,t)\in L^\infty(\Omega_{\rm H})$, $V_{\rm m}(\cdot,t)\in H^1(\Omega_{\rm H})$ and $u_{\rm e}(\cdot,t)\in H^1(\Omega_{\rm H})\cap L^2_0(\Omega_{\rm H})$, such that

$$\begin{aligned} \int_{\Omega_{\rm H}}\big(\partial_t w + g(V_{\rm m},w)\big)\xi = 0, \\ \chi_{\rm m}\int_{\Omega_{\rm H}}\big(\partial_t V_{\rm m} + I_{\rm ion}(V_{\rm m},w)\big)\phi + \int_{\Omega_{\rm H}}\boldsymbol{\sigma}_{\rm i}\boldsymbol{\nabla}(V_{\rm m}+u_{\rm e})\cdot\boldsymbol{\nabla}\phi = \int_{\Omega_{\rm H}} I_{\rm app}\phi, \\ \int_{\Omega_{\rm H}}(\boldsymbol{\sigma}_{\rm i}+\boldsymbol{\sigma}_{\rm e})\boldsymbol{\nabla}u_{\rm e}\cdot\boldsymbol{\nabla}\psi + \int_{\Omega_{\rm H}}\boldsymbol{\sigma}_{\rm i}\boldsymbol{\nabla}V_{\rm m}\cdot\boldsymbol{\nabla}\psi = 0, \end{aligned} \tag{3.19}$$

for all $(\xi,\phi,\psi)\in L^2(\Omega_{\rm H})\times H^1(\Omega_{\rm H})\times\big(H^1(\Omega_{\rm H})\cap L^2_0(\Omega_{\rm H})\big)$.

3.2 Time semi-discrete formulations: decoupled time-marching schemes

Let $N\in\mathbb{N}^*$ be a given integer and consider a uniform partition $\{[t_n,t_{n+1}]\}_{0\le n\le N-1}$, with $t_n\stackrel{\rm def}{=}n\tau$, of the time interval of interest $(0,T)$, with time-step $\tau\stackrel{\rm def}{=}T/N$.

For a given time dependent function X, the quantity X^n denotes an approximation of $X(t_n)$ and $D_\tau X^n \stackrel{\text{def}}{=} (X^n - X^{n-1})/\tau$ the first order backward difference. Moreover, we set $I^n_{\text{app}} \stackrel{\text{def}}{=} I_{\text{app}}(t_n, \cdot)$.

We propose to time semi-discretize (3.19) by combining a first order semi-implicit treatment of the ionic current evaluation with an explicit (Gauss-Seidel or Jacobi like) treatment of the coupling between V_{m} and u_{e}. The resulting schemes can be cast into a common frame as follows: For $0 \leq n \leq N-1$, we solve

1. Ionic state: find $w^{n+1} \in L^\infty(\Omega_{\text{H}})$ such that

$$\int_{\Omega_{\text{H}}} \big(D_\tau w^{n+1} + g(V^n_{\text{m}}, w^{n+1})\big)\xi = 0 \tag{3.20}$$

   for all $\xi \in L^2(\Omega_{\text{H}})$.

2. Transmembrane potential: find $V^{n+1}_{\text{m}} \in H^1(\Omega_{\text{H}})$ such that

$$\chi_{\text{m}} \int_{\Omega_{\text{H}}} D_\tau V^{n+1}_{\text{m}} \phi + \int_{\Omega_{\text{H}}} \boldsymbol{\sigma}_{\text{i}} \boldsymbol{\nabla} V^{n+1}_{\text{m}} \cdot \boldsymbol{\nabla}\phi + \int_{\Omega_{\text{H}}} \boldsymbol{\sigma}_{\text{i}} \boldsymbol{\nabla} u^\star_{\text{e}} \cdot \boldsymbol{\nabla}\phi = \int_{\Omega_{\text{H}}} \big(I^{n+1}_{\text{app}} - I_{\text{ion}}(V^n_{\text{m}}, w^{n+1})\big)\,\phi \tag{3.21}$$

   for all $\phi \in H^1(\Omega_{\text{H}})$.

3. Extracellular potential: find $u^{n+1}_{\text{e}} \in H^1(\Omega_{\text{H}}) \cap L^2_0(\Omega_{\text{H}})$,

$$\int_{\Omega_{\text{H}}} (\boldsymbol{\sigma}_{\text{i}} + \boldsymbol{\sigma}_{\text{e}}) \boldsymbol{\nabla} u^{n+1}_{\text{e}} \cdot \boldsymbol{\nabla}\psi + \int_{\Omega_{\text{H}}} \boldsymbol{\sigma}_{\text{i}} \boldsymbol{\nabla} V^\star_{\text{m}} \cdot \boldsymbol{\nabla}\psi = 0 \tag{3.22}$$

   for all $\psi \in H^1(\Omega_{\text{H}}) \cap L^2_0(\Omega_{\text{H}})$.

Note that the non-linear system (3.20) and the ionic current evaluation $I_{\text{ion}}(V^n_{\text{m}}, w^{n+1})$ in (3.21) are decoupled from (3.21)-(3.22). This semi-implicit treatment is quite popular in the literature (see *e.g.* [43, 30, 14, 2, 5, 19]). For $(u^\star_{\text{e}}, V^\star_{\text{m}}) = (u^{n+1}_{\text{e}}, V^{n+1}_{\text{m}})$, the unknown potentials V^{n+1}_{m} and u^{n+1}_{e} are implicit coupled and, therefore, equations (3.21) and (3.22) have to be solved simultaneously (see *e.g.* [26, 44, 19, 19, 4]). The energy based stability analysis of this semi-implicit scheme, using first and second order time discretizations, has been recently reported in [19].

On the contrary, for $(u^\star_{\text{e}}, V^\star_{\text{m}}) = (u^n_{\text{e}}, V^{n+1}_{\text{m}})$ or $(u^\star_{\text{e}}, V^\star_{\text{m}}) = (u^n_{\text{e}}, V^n_{\text{m}})$, the electrodiffusive coupling becomes explicit and therefore (3.21) and (3.22) can be solved separately: either sequentially (Gauss-Seidel) or in parallel (Jacobi). Similar Gauss-Seidel like splittings have been proposed and successfully applied in [43, 30, 2, 48]. The theoretical stability of the schemes is, however, not established therein. To the best of our knowledge, the Jacobi like splitting has not yet been considered in the literature.

The energy based stability analysis of these time splitting schemes is performed in the next subsection.

Remark 3.1 *The Gauss-Seidel and Jacobi like electrodiffusive splittings allow a decoupled computation of* V_{m} *and* u_{e} *without the need to resort to monodomain approximations (see Remark 2.1).*

3.3 Stability analysis

For the stability analysis below, we shall make use of the following simplifying assumption (see [19, Section 3.2.2] and Remark 3.1 therein) on the structure of the ionic functions g and $I_{\rm ion}$:

$$\begin{aligned} I_{\rm ion}(V_{\rm m},w) &\le C_I\big(|V_{\rm m}|+|w|\big),\\ g(V_{\rm m},w) &\le C_g\big(|V_{\rm m}|+|w|\big) \end{aligned} \tag{3.23}$$

for all $V_{\rm m}, w$, and we set $\alpha \stackrel{\rm def}{=} 1+3C_I+C_g$ and $\beta \stackrel{\rm def}{=} C_I+3C_g$.

The next theorem states the energy based stability of the time-marching schemes (3.20)-(3.22), in terms of $u_{\rm e}^\star$ and $V_{\rm m}^\star$.

Theorem 3.2 *Assume that* (3.23) *holds and that the conductivity tensors* $\boldsymbol{\sigma}_{\rm i}, \boldsymbol{\sigma}_{\rm e}$ *are symmetric and positive-definite. Let* $\{(w^n, V_{\rm m}^n, u_{\rm e}^n)\}_{n=0}^N$ *be solution of* (3.20)-(3.22) *and* $C(T,\alpha,\beta) \stackrel{\rm def}{=} \exp\big(T/(1-\tau\max\{\alpha,\beta\})\big)$. *Then, under the condition*

$$\tau < \frac{1}{\max\{\alpha,\beta\}}, \tag{3.24}$$

there follows:

- *For* $(u_{\rm e}^\star, V_{\rm m}^\star) = (u_{\rm e}^{n+1}, V_{\rm m}^{n+1})$*:*

$$\begin{aligned} &\big\|w^n\big\|_{0,\Omega_{\rm H}}^2 + \chi_{\rm m}\big\|V_{\rm m}^n\big\|_{0,\Omega_{\rm H}}^2 \\ &\quad + 2\sum_{m=0}^{n-1}\tau\big\|\boldsymbol{\sigma}_{\rm e}^{\frac12}\boldsymbol{\nabla}u_{\rm e}^{m+1}\big\|_{0,\Omega_{\rm H}}^2 + 2\sum_{m=0}^{n-1}\tau\big\|\boldsymbol{\sigma}_{\rm i}^{\frac12}\boldsymbol{\nabla}(V_{\rm m}^{m+1}+u_{\rm e}^{m+1})\big\|_{0,\Omega_{\rm H}}^2 \\ &\le C(T,\alpha,\beta)\left(\big\|w^0\big\|_{0,\Omega_{\rm H}}^2 + \chi_{\rm m}\big\|V_{\rm m}^0\big\|_{0,\Omega_{\rm H}}^2 + \sum_{m=0}^{n-1}\tau\big\|I_{\rm app}^{m+1}\big\|_{0,\Omega_{\rm H}}^2\right), \end{aligned} \tag{3.25}$$

  with $1\le n\le N$.

- *For* $(u_{\rm e}^\star, V_{\rm m}^\star) = (u_{\rm e}^{n}, V_{\rm m}^{n+1})$*:*

$$\begin{aligned} &\big\|w^n\big\|_{0,\Omega_{\rm H}}^2 + \chi_{\rm m}\big\|V_{\rm m}^n\big\|_{0,\Omega_{\rm H}}^2 + \tau\big\|\boldsymbol{\sigma}_{\rm i}^{\frac12}\boldsymbol{\nabla}u_{\rm e}^n\big\|_{0,\Omega_{\rm H}}^2 \\ &\quad + 2\sum_{m=0}^{n-1}\tau\big\|\boldsymbol{\sigma}_{\rm e}^{\frac12}\boldsymbol{\nabla}u_{\rm e}^{m+1}\big\|_{0,\Omega_{\rm H}}^2 + \sum_{m=0}^{n-1}\tau\big\|\boldsymbol{\sigma}_{\rm i}^{\frac12}\boldsymbol{\nabla}(V_{\rm m}^{m+1}+u_{\rm e}^{m+1})\big\|_{0,\Omega_{\rm H}}^2 \\ &\le C(T,\alpha,\beta)\left(\big\|w^0\big\|_{0,\Omega_{\rm H}}^2 + \chi_{\rm m}\big\|V_{\rm m}^0\big\|_{0,\Omega_{\rm H}}^2 + \tau\big\|\boldsymbol{\sigma}_{\rm i}^{\frac12}\boldsymbol{\nabla}u_{\rm e}^0\big\|_{0,\Omega_{\rm H}}^2 + \sum_{m=0}^{n-1}\tau\big\|I_{\rm app}^{m+1}\big\|_{0,\Omega_{\rm H}}^2\right), \end{aligned} \tag{3.26}$$

  with $1\le n\le N$.

- *For* $(u_{\rm e}^\star, V_{\rm m}^\star) = (u_{\rm e}^n, V_{\rm m}^n)$*:*

$$\begin{aligned}
&\big\|w^n\big\|_{0,\Omega_{\rm H}}^2 + \chi_{\rm m}\big\|V_{\rm m}^n\big\|_{0,\Omega_{\rm H}}^2 \\
&\quad + \tau\big\|\boldsymbol{\sigma}_{\rm i}^{\frac{1}{2}}\boldsymbol{\nabla} u_{\rm e}^n\big\|_{0,\Omega_{\rm H}}^2 + \tau\big\|\boldsymbol{\sigma}_{\rm i}^{\frac{1}{2}}\boldsymbol{\nabla} V_{\rm m}^n\big\|_{0,\Omega_{\rm H}}^2 + 2\sum_{m=0}^{n-1}\tau\big\|\boldsymbol{\sigma}_{\rm e}^{\frac{1}{2}}\boldsymbol{\nabla} u_{\rm e}^{m+1}\big\|_{0,\Omega_{\rm H}}^2 \\
&\qquad \le C(T,\alpha,\beta)\left(\big\|w^0\big\|_{0,\Omega_{\rm H}}^2 + \chi_{\rm m}\big\|V_{\rm m}^0\big\|_{0,\Omega_{\rm H}}^2 + \tau\big\|\boldsymbol{\sigma}_{\rm i}^{\frac{1}{2}}\boldsymbol{\nabla} V_{\rm m}^0\big\|_{0,\Omega_{\rm H}}^2\right. \\
&\qquad\qquad \left. +\tau\big\|\boldsymbol{\sigma}_{\rm i}^{\frac{1}{2}}\boldsymbol{\nabla} u_{\rm e}^0\big\|_{0,\Omega_{\rm H}}^2 + \sum_{m=0}^{n-1}\tau\big\|I_{\rm app}^{m+1}\big\|_{0,\Omega_{\rm H}}^2\right), \quad (3.27)
\end{aligned}$$

with $1 \le n \le N$.

Proof. Under assumptions (3.23) and (3.24), the stability estimate (3.25), for the monolithic case $(u_{\rm e}^\star, V_{\rm m}^\star) = (u_{\rm e}^{n+1}, V_{\rm m}^{n+1})$, can be straightforwardly derived from the analysis reported in [19] (see also [45]). Therefore, we only detail here the proofs of (3.26) and (3.27).

Let first consider the Gauss-Seidel like decoupling $(u_{\rm e}^\star, V_{\rm m}^\star) = (u_{\rm e}^n, V_{\rm m}^{n+1})$. By testing (3.20)-(3.22) with $\tau(w^{n+1}, V_{\rm m}^{n+1}, u_{\rm e}^{n+1})$ and after summation of the resulting expressions we have:

$$\begin{aligned}
&\frac{1}{2}\left(\big\|w^{n+1}\big\|_{0,\Omega_{\rm H}}^2 - \big\|w^n\big\|_{0,\Omega_{\rm H}}^2\right) + \frac{\chi_{\rm m}}{2}\left(\big\|V_{\rm m}^{n+1}\big\|_{0,\Omega_{\rm H}}^2 - \big\|V_{\rm m}^n\big\|_{0,\Omega_{\rm H}}^2\right) + \tau\big\|\boldsymbol{\sigma}_{\rm e}^{\frac{1}{2}}\boldsymbol{\nabla} u_{\rm e}^{n+1}\big\|_{0,\Omega_{\rm H}}^2 \\
&\quad + \tau\big\|\boldsymbol{\sigma}_{\rm i}^{\frac{1}{2}}\boldsymbol{\nabla}(V_{\rm m}^{n+1} + u_{\rm e}^{n+1})\big\|_{0,\Omega_{\rm H}}^2 + \underbrace{\tau\int_{\Omega_{\rm H}}\boldsymbol{\sigma}_{\rm i}\boldsymbol{\nabla}(u_{\rm e}^n - u_{\rm e}^{n+1})\cdot\boldsymbol{\nabla} V_{\rm m}^{n+1}}_{I_1} \\
&\le \underbrace{\tau\int_{\Omega_{\rm H}}\left(I_{\rm app}^{n+1} - I_{\rm ion}(V_{\rm m}^n, w^{n+1})\right)V_{\rm m}^{n+1} - \tau\int_{\Omega_{\rm H}} g(V_{\rm m}^n, w^{n+1}))w^{n+1}}_{I_2}, \quad (3.28)
\end{aligned}$$

where the square roots $\boldsymbol{\sigma}_{\rm e}^{\frac{1}{2}}, \boldsymbol{\sigma}_{\rm i}^{\frac{1}{2}}$ are well defined since $\boldsymbol{\sigma}_{\rm i}, \boldsymbol{\sigma}_{\rm e}$ are symmetric and positive-definite tensors (see *e.g.* [40]). We now provide appropriate bounds for terms I_1 and I_2.

As regards the first term, we have

$$\begin{aligned}
I_1 =& \tau\int_{\Omega_{\rm H}}\boldsymbol{\sigma}_{\rm i}\boldsymbol{\nabla}(u_{\rm e}^n - u_{\rm e}^{n+1})\cdot\boldsymbol{\nabla}(V_{\rm m}^{n+1} + u_{\rm e}^{n+1}) + \int_{\Omega_{\rm H}}\boldsymbol{\sigma}_{\rm i}\boldsymbol{\nabla}(u_{\rm e}^{n+1} - u_{\rm e}^n)\cdot\boldsymbol{\nabla} u_{\rm e}^{n+1} \\
\ge& -\frac{\tau}{2}\big\|\boldsymbol{\sigma}_{\rm i}^{\frac{1}{2}}\boldsymbol{\nabla}(u_{\rm e}^n - u_{\rm e}^{n+1})\big\|_{0,\Omega_{\rm H}}^2 - \frac{\tau}{2}\big\|\boldsymbol{\sigma}_{\rm i}^{\frac{1}{2}}\boldsymbol{\nabla}(V_{\rm m}^{n+1} + u_{\rm e}^{n+1})\big\|_{0,\Omega_{\rm H}}^2 \\
&+ \frac{\tau}{2}\left(\big\|\boldsymbol{\sigma}_{\rm i}^{\frac{1}{2}}\boldsymbol{\nabla} u_{\rm e}^{n+1}\big\|_{0,\Omega_{\rm H}}^2 - \big\|\boldsymbol{\sigma}_{\rm i}^{\frac{1}{2}}\boldsymbol{\nabla} u_{\rm e}^n\big\|_{0,\Omega_{\rm H}}^2\right) + \frac{\tau}{2}\big\|\boldsymbol{\sigma}_{\rm i}^{\frac{1}{2}}\boldsymbol{\nabla}(u_{\rm e}^{n+1} - u_{\rm e}^n)\big\|_{0,\Omega_{\rm H}}^2 \\
=& \frac{\tau}{2}\left(\big\|\boldsymbol{\sigma}_{\rm i}^{\frac{1}{2}}\boldsymbol{\nabla} u_{\rm e}^{n+1}\big\|_{0,\Omega_{\rm H}}^2 - \big\|\boldsymbol{\sigma}_{\rm i}^{\frac{1}{2}}\boldsymbol{\nabla} u_{\rm e}^n\big\|_{0,\Omega_{\rm H}}^2\right) - \frac{\tau}{2}\big\|\boldsymbol{\sigma}_{\rm i}^{\frac{1}{2}}\boldsymbol{\nabla}(V_{\rm m}^{n+1} + u_{\rm e}^{n+1})\big\|_{0,\Omega_{\rm H}}^2. \quad (3.29)
\end{aligned}$$

On the other hand, from (3.23), for the second term can be bounded as follows

$$\begin{aligned} I_2 =& \frac{\tau}{2}\big\|I_{\rm app}^{n+1}\big\|^2_{0,\Omega_{\rm H}{}^2} + \frac{\tau}{2}\big\|V_{\rm m}^{n+1}\big\|^2_{0,\Omega_{\rm H}} + \frac{\tau C_I}{2}\left(3\big\|V_{\rm m}^{n+1}\big\|^2_{0,\Omega_{\rm H}} + \big\|w^{n+1}\big\|^2_{0,\Omega_{\rm H}}\right) \\ &+ \frac{\tau C_g}{2}\left(\big\|V_{\rm m}^{n+1}\big\|^2_{0,\Omega_{\rm H}} + 3\big\|w^{n+1}\big\|^2_{0,\Omega_{\rm H}}\right) \\ =& \frac{\tau}{2}\big\|I_{\rm app}^{n+1}\big\|^2_{0,\Omega_{\rm H}} + \frac{\tau}{2}\underbrace{(1+3C_I+C_g)}_{\alpha}\big\|V_{\rm m}^{n+1}\big\|^2_{0,\Omega_{\rm H}} + \frac{\tau}{2}\underbrace{(C_I+3C_g)}_{\beta}\big\|w^{n+1}\big\|^2_{0,\Omega_{\rm H}}. \end{aligned} \tag{3.30}$$

As a result, inserting (3.29) and (3.30) into (3.28), yields

$$\begin{aligned} &\frac{1}{2}\left(\big\|w^{n+1}\big\|^2_{0,\Omega_{\rm H}} - \big\|w^{n}\big\|^2_{0,\Omega_{\rm H}}\right) + \frac{\chi_{\rm m}}{2}\left(\big\|V_{\rm m}^{n+1}\big\|^2_{0,\Omega_{\rm H}} - \big\|V_{\rm m}^{n}\big\|^2_{0,\Omega_{\rm H}}\right) + \tau\big\|\boldsymbol{\sigma}_{\rm e}^{\frac{1}{2}}\boldsymbol{\nabla} u_{\rm e}^{n+1}\big\|^2_{0,\Omega_{\rm H}} \\ &+ \frac{\tau}{2}\big\|\boldsymbol{\sigma}_{\rm i}^{\frac{1}{2}}\boldsymbol{\nabla}(V_{\rm m}^{n+1}+u_{\rm e}^{n+1})\big\|^2_{0,\Omega_{\rm H}} + \frac{\tau}{2}\left(\big\|\boldsymbol{\sigma}_{\rm i}^{\frac{1}{2}}\boldsymbol{\nabla} u_{\rm e}^{n+1}\big\|^2_{0,\Omega_{\rm H}} - \big\|\boldsymbol{\sigma}_{\rm i}^{\frac{1}{2}}\boldsymbol{\nabla} u_{\rm e}^{n}\big\|^2_{0,\Omega_{\rm H}}\right) \\ &\qquad \le \frac{\tau}{2}\big\|I_{\rm app}^{n+1}\big\|^2_{0,\Omega_{\rm H}} + \frac{\tau\alpha}{2}\big\|V_{\rm m}^{n+1}\big\|^2_{0,\Omega_{\rm H}} + \frac{\tau\beta}{2}\big\|w^{n+1}\big\|^2_{0,\Omega_{\rm H}}, \end{aligned}$$

so that, replacing index n by m and summing over $0 \le m \le n-1$, we have

$$\begin{aligned} &\big\|w^{n}\big\|^2_{0,\Omega_{\rm H}} + \chi_{\rm m}\big\|V_{\rm m}^{n}\big\|^2_{0,\Omega_{\rm H}} + \tau\big\|\boldsymbol{\sigma}_{\rm i}^{\frac{1}{2}}\boldsymbol{\nabla} u_{\rm e}^{n}\big\|^2_{0,\Omega_{\rm H}} + 2\sum_{m=0}^{n-1}\tau\big\|\boldsymbol{\sigma}_{\rm e}^{\frac{1}{2}}\boldsymbol{\nabla} u_{\rm e}^{m+1}\big\|^2_{0,\Omega_{\rm H}} \\ &+\sum_{m=0}^{n-1}\tau\big\|\boldsymbol{\sigma}_{\rm i}^{\frac{1}{2}}\boldsymbol{\nabla}(V_{\rm m}^{m+1}+u_{\rm e}^{m+1})\big\|^2_{0,\Omega_{\rm H}} \le \big\|w^{0}\big\|^2_{0,\Omega_{\rm H}} + \chi_{\rm m}\big\|V_{\rm m}^{0}\big\|^2_{0,\Omega_{\rm H}} + \tau\big\|\boldsymbol{\sigma}_{\rm i}^{\frac{1}{2}}\boldsymbol{\nabla} u_{\rm e}^{0}\big\|^2_{0,\Omega_{\rm H}} \\ &\qquad + \sum_{m=0}^{n-1}\tau\big\|I_{\rm app}^{m+1}\big\|^2_{0,\Omega_{\rm H}} + \alpha\sum_{m=0}^{n-1}\tau\big\|V_{\rm m}^{m+1}\big\|^2_{0,\Omega_{\rm H}} + \beta\sum_{m=0}^{n-1}\tau\big\|w^{m+1}\big\|^2_{0,\Omega_{\rm H}}. \end{aligned}$$

Estimate (3.26) then follows by applying Gronwall's lemma (see *e.g.* [23, Lemma 5.1]) under condition (3.24).

Finally, let consider the Jacobi like decoupling $(u_{\rm e}^\star, V_{\rm m}^\star) = (u_{\rm e}^n, V_{\rm m}^n)$. In this case, estimate (3.28) becomes

$$\begin{aligned} &\frac{1}{2}\left(\big\|w^{n+1}\big\|^2_{0,\Omega_{\rm H}} - \big\|w^{n}\big\|^2_{0,\Omega_{\rm H}}\right) + \frac{\chi_{\rm m}}{2}\left(\big\|V_{\rm m}^{n+1}\big\|^2_{0,\Omega_{\rm H}} - \big\|V_{\rm m}^{n}\big\|^2_{0,\Omega_{\rm H}}\right) + \tau\big\|\boldsymbol{\sigma}_{\rm e}^{\frac{1}{2}}\boldsymbol{\nabla} u_{\rm e}^{n+1}\big\|^2_{0,\Omega_{\rm H}} \\ &+ \tau\big\|\boldsymbol{\sigma}_{\rm i}^{\frac{1}{2}}\boldsymbol{\nabla}(V_{\rm m}^{n+1}+u_{\rm e}^{n+1})\big\|^2_{0,\Omega_{\rm H}} + I_1 + \underbrace{\tau\int_{\Omega_{\rm H}}\boldsymbol{\sigma}_{\rm i}\boldsymbol{\nabla}(V_{\rm m}^{n}-V_{\rm m}^{n+1})\cdot\boldsymbol{\nabla} u_{\rm e}^{n+1}}_{I_3} \le I_2. \end{aligned} \tag{3.31}$$

The new term I_3 can be bounded similarly to I_1, that is,

$$\begin{aligned} I_3 =& \tau\int_{\Omega_{\rm H}}\boldsymbol{\sigma}_{\rm i}\boldsymbol{\nabla}(V_{\rm m}^{n}-V_{\rm m}^{n+1})\cdot\boldsymbol{\nabla}(V_{\rm m}^{n+1}+u_{\rm e}^{n+1}) + \int_{\Omega_{\rm H}}\boldsymbol{\sigma}_{\rm i}\boldsymbol{\nabla}(V_{\rm m}^{n+1}-V_{\rm m}^{n})\cdot\boldsymbol{\nabla} V_{\rm m}^{n+1} \\ \ge& -\frac{\tau}{2}\big\|\boldsymbol{\sigma}_{\rm i}^{\frac{1}{2}}\boldsymbol{\nabla}(V_{\rm m}^{n}-V_{\rm m}^{n+1})\big\|^2_{0,\Omega_{\rm H}} - \frac{\tau}{2}\big\|\boldsymbol{\sigma}_{\rm i}^{\frac{1}{2}}\boldsymbol{\nabla}(V_{\rm m}^{n+1}+u_{\rm e}^{n+1})\big\|^2_{0,\Omega_{\rm H}} \\ &+ \frac{\tau}{2}\left(\big\|\boldsymbol{\sigma}_{\rm i}^{\frac{1}{2}}\boldsymbol{\nabla} V_{\rm m}^{n+1}\big\|^2_{0,\Omega_{\rm H}} - \big\|\boldsymbol{\sigma}_{\rm i}^{\frac{1}{2}}\boldsymbol{\nabla} V_{\rm m}^{n}\big\|^2_{0,\Omega_{\rm H}}\right) + \frac{\tau}{2}\big\|\boldsymbol{\sigma}_{\rm i}^{\frac{1}{2}}\boldsymbol{\nabla}(V_{\rm m}^{n+1}-V_{\rm m}^{n})\big\|^2_{0,\Omega_{\rm H}} \\ =& \frac{\tau}{2}\left(\big\|\boldsymbol{\sigma}_{\rm i}^{\frac{1}{2}}\boldsymbol{\nabla} V_{\rm m}^{n+1}\big\|^2_{0,\Omega_{\rm H}} - \big\|\boldsymbol{\sigma}_{\rm i}^{\frac{1}{2}}\boldsymbol{\nabla} V_{\rm m}^{n}\big\|^2_{0,\Omega_{\rm H}}\right) - \frac{\tau}{2}\big\|\boldsymbol{\sigma}_{\rm i}^{\frac{1}{2}}\boldsymbol{\nabla}(V_{\rm m}^{n+1}+u_{\rm e}^{n+1})\big\|^2_{0,\Omega_{\rm H}}. \end{aligned} \tag{3.32}$$

Therefore, by inserting (3.29), (3.30) and (3.32) into (3.31), there follows that

$$\frac{1}{2}\left(\left\|w^{n+1}\right\|_{0,\Omega_{\mathrm{H}}}^2-\left\|w^{n}\right\|_{0,\Omega_{\mathrm{H}}}^2\right)+\frac{\chi_{\mathrm{m}}}{2}\left(\left\|V_{\mathrm{m}}^{n+1}\right\|_{0,\Omega_{\mathrm{H}}}^2-\left\|V_{\mathrm{m}}^{n}\right\|_{0,\Omega_{\mathrm{H}}}^2\right)+\tau\left\|\boldsymbol{\sigma}_{\mathrm{e}}^{\frac{1}{2}}\boldsymbol{\nabla}u_{\mathrm{e}}^{n+1}\right\|_{0,\Omega_{\mathrm{H}}}^2$$
$$\frac{\tau}{2}\left(\left\|\boldsymbol{\sigma}_{\mathrm{i}}^{\frac{1}{2}}\boldsymbol{\nabla}V_{\mathrm{m}}^{n+1}\right\|_{0,\Omega_{\mathrm{H}}}^2-\left\|\boldsymbol{\sigma}_{\mathrm{i}}^{\frac{1}{2}}\boldsymbol{\nabla}V_{\mathrm{m}}^{n}\right\|_{0,\Omega_{\mathrm{H}}}^2\right)+\frac{\tau}{2}\left(\left\|\boldsymbol{\sigma}_{\mathrm{i}}^{\frac{1}{2}}\boldsymbol{\nabla}u_{\mathrm{e}}^{n+1}\right\|_{0,\Omega_{\mathrm{H}}}^2-\left\|\boldsymbol{\sigma}_{\mathrm{i}}^{\frac{1}{2}}\boldsymbol{\nabla}u_{\mathrm{e}}^{n}\right\|_{0,\Omega_{\mathrm{H}}}^2\right)$$
$$\leq\frac{\tau}{2}\left\|I_{\mathrm{app}}^{n+1}\right\|_{0,\Omega_{\mathrm{H}}}^2+\frac{\tau\alpha}{2}\left\|V_{\mathrm{m}}^{n+1}\right\|_{0,\Omega_{\mathrm{H}}}^2+\frac{\tau\beta}{2}\left\|w^{n+1}\right\|_{0,\Omega_{\mathrm{H}}}^2.$$

Estimate (3.27) then holds, under condition (3.24), by replacing index n by m, summing over $0\leq m\leq n-1$ and applying Gronwall's lemma. This completes the proof.

We conclude this section with a series of remarks.

Remark 3.3 *Theorem 3.2 shows that electrodiffusive Gauss-Seidel and Jacobi splittings are energy stable under condition* (3.24)*, as for the unsplit case* $(u_{\mathrm{e}}^{\star},V_{\mathrm{m}}^{\star})=(u_{\mathrm{e}}^{n+1},V_{\mathrm{m}}^{n+1})$ *(analyzed in [19]), but with slightly altered energy norms. As a result, stability is not compromised.*

Remark 3.4 *The proof of Theorem 3.2 does not depend on the time discretizations considered in* (3.20) *and* (3.21)*. Indeed, we do not make use of any numerical dissipation produced by the scheme, a part from that is directly provided by the splitting. Therefore, the backward Euler quotients,* $D_\tau w^{n+1}$ *and* $D_\tau V_{\mathrm{m}}^{n+1}$*, can be safely replaced by a second order backward difference formula, and perform one correction (see e.g. [41, 39]) to recover overall second order accuracy.*

Remark 3.5 *The above stability result can be adapted, with minor modifications, to the case* $(u_{\mathrm{e}}^{\star},V_{\mathrm{m}}^{\star})=(u_{\mathrm{e}}^{n+1},V_{\mathrm{m}}^{n})$*. The full Jacobi splitting, obtained after replacing* $I_{\mathrm{ion}}(V_{\mathrm{m}}^{n},w^{n+1})$ *by* $I_{\mathrm{ion}}(V_{\mathrm{m}}^{n},w^{n})$ *in* (3.21) *could also be considered.*

Remark 3.6 *Theorem 3.2 holds also for the fully discrete counterpart of* (3.20)-(3.22) *obtained by discretizing in space using finite elements (see subsection §4.1).*

4 Decoupled time-marching for ECG numerical simulation

In this section, we introduce fully discrete schemes for the heart-torso system (2.8)-(2.16), allowing a decoupled computation of the transmembrane, extracellular and torso potentials. The main idea consists in combining the bidomain spplitings of the previous section, with a specific explicit Robin-Robin treatment of the heart-torso coupling conditions (2.14)-(2.15).

4.1 Preliminaries

Problem (2.8)-(2.16) can be cast into weak form as follows (see *e.g.* [6]): for $t>0$, find $w(\cdot,t)\in L^{\infty}(\Omega_{\mathrm{H}})$, $V_{\mathrm{m}}(\cdot,t)\in H^1(\Omega_{\mathrm{H}})$, $u_{\mathrm{e}}(\cdot,t)\in H^1(\Omega_{\mathrm{H}})\cap L_0^2(\Omega_{\mathrm{H}})$

and $u_{\rm T}(\cdot,t) \in H^1(\Omega_{\rm T})$ with $u_{\rm e}(\cdot,t) = u_{\rm T}(\cdot,t)$ on Σ, such that

$$\begin{aligned}
\int_{\Omega_{\rm H}} \big(\partial_t w + g(V_{\rm m},w)\big)\xi = 0,\\
\chi_{\rm m}\int_{\Omega_{\rm H}} \big(\partial_t V_{\rm m} + I_{\rm ion}(V_{\rm m},w)\big)\phi + \int_{\Omega_{\rm H}} \boldsymbol{\sigma}_{\rm i}\boldsymbol{\nabla}(V_{\rm m}+u_{\rm e})\cdot\boldsymbol{\nabla}\phi = \int_{\Omega_{\rm H}} I_{\rm app}\phi,\\
\int_{\Omega_{\rm H}} (\boldsymbol{\sigma}_{\rm i}+\boldsymbol{\sigma}_{\rm e})\boldsymbol{\nabla}u_{\rm e}\cdot\boldsymbol{\nabla}\psi + \int_{\Omega_{\rm H}} \boldsymbol{\sigma}_{\rm i}\boldsymbol{\nabla}V_{\rm m}\cdot\boldsymbol{\nabla}\psi + \int_{\Omega_{\rm T}} \boldsymbol{\sigma}_{\rm T}\boldsymbol{\nabla}u_{\rm T}\cdot\boldsymbol{\nabla}\zeta = 0,
\end{aligned} \tag{4.33}$$

for all $(\xi,\phi,\psi,\zeta) \in L^2(\Omega_{\rm H}) \times H^1(\Omega_{\rm H}) \times \big(H^1(\Omega_{\rm H}) \cap L^2_0(\Omega_{\rm H})\big) \times H^1(\Omega_{\rm T})$ with $\psi = \zeta$ on Σ.

Assume that $\Omega_{\rm H}$ and $\Omega_{\rm T}$ are polygonal domains and let $\{\mathcal{T}_{{\rm H},h}\}_{0<h\leq 1}$ ($\{\mathcal{T}_{{\rm T},h}\}_{0<h\leq 1}$) be a family of triangulations of $\Omega_{\rm H}$ (resp. $\Omega_{\rm T}$) satisfying the usual requirements of finite element approximations (see *e.g.* [18]). The subscript $h \in (0,1]$ refer to the level of refinement of the triangulations. For the sake of simplicity and without loss of generality, we assume that both families of triangulations are quasi-uniform and that they match at the heart-torso interface Σ. We define $X_{{\rm H},h}$ (resp. $X_{{\rm T},h}$) as an internal continuous Lagrange finite element approximation of $H^1(\Omega_{\rm H})$ (resp. $H^1(\Omega_{\rm T})$). We also introduce the standard finite element (heart-to-torso) lifting operator $\mathcal{L}_h : X_{{\rm H},h} \to X_{{\rm T},h} \cap H^1_{\Gamma_{\rm ext}}(\Omega_{\rm T})$, such that $\mathcal{L}_h\psi = \psi$ on Σ and $\mathcal{L}_h\psi = 0$ on $\Gamma_{\rm ext}$, for all $\psi \in X_{{\rm H},h}$. Note that we have the direct sum decomposition

$$\begin{aligned}
\big\{(\psi,\zeta) \in X_{{\rm H},h}\times X_{{\rm T},h} \,:\, \psi_{|\Sigma} = \zeta_{|\Sigma}\big\} = &\big\{\big(\psi,\mathcal{L}_h\psi\big) \,:\, \psi \in X_{{\rm H},h}\big\}\\
&\oplus \big\{(0,\zeta) \,:\, \zeta \in X_{{\rm T},h} \cap H^1_\Sigma(\Omega_{\rm T})\big\}.
\end{aligned} \tag{4.34}$$

In the stability analysis below, we shall make use of the following standard discrete trace-inverse inequality (see *e.g.* [45]):

$$||v||^2_{0,\partial K} \leq \frac{C_{\rm ti}}{h}||v||^2_{0,K} \quad \forall v \in X_{{\rm T},h}, \tag{4.35}$$

for all $K \in \mathcal{T}_{{\rm T},h}$, and with $C_{\rm ti} > 0$ a constant independent of the discretization parameter h (but that might depend on the polynomial order).

By combining the semi-implicit time-marching schemes of section §3 with a finite element discretization in space, we can derive from (4.33) the following fully discrete heart-torso scheme: for $0 \leq n \leq N-1$, find $w^{n+1} \in X_{{\rm H},h}$, $V_{\rm m}^{n+1} \in X_{{\rm H},h}$, $u_{\rm e}^{n+1} \in X_{{\rm H},h} \cap L^2_0(\Omega_{\rm H})$ and $u_{\rm T}^{n+1} \in X_{{\rm T},h}$ with $u_{\rm T}^{n+1} = u_{\rm e}^{n+1}$ on Σ, such that

$$\int_{\Omega_{\rm H}} \big(D_\tau w^{n+1} + g(V_{\rm m}^n, w^{n+1})\big)\xi = 0, \tag{4.36}$$

$$\chi_{\rm m}\int_{\Omega_{\rm H}} D_\tau V_{\rm m}^{n+1}\phi + \int_{\Omega_{\rm H}} \boldsymbol{\sigma}_{\rm i}\boldsymbol{\nabla}(V_{\rm m}^{n+1}+u_{\rm e}^\star)\cdot\boldsymbol{\nabla}\phi = \int_{\Omega_{\rm H}} \big(I_{\rm app}^{n+1} - I_{\rm ion}(V_{\rm m}^n, w^{n+1})\big)\phi, \tag{4.37}$$

$$\int_{\Omega_{\rm H}} (\boldsymbol{\sigma}_{\rm i}+\boldsymbol{\sigma}_{\rm e})\boldsymbol{\nabla}u_{\rm e}^{n+1}\cdot\boldsymbol{\nabla}\psi + \int_{\Omega_{\rm H}} \boldsymbol{\sigma}_{\rm i}\boldsymbol{\nabla}V_{\rm m}^\star\cdot\boldsymbol{\nabla}\psi + \int_{\Omega_{\rm T}} \boldsymbol{\sigma}_{\rm T}\boldsymbol{\nabla}u_{\rm T}^{n+1}\cdot\boldsymbol{\nabla}\zeta = 0, \tag{4.38}$$

for all $(\xi, \phi, \psi, \zeta) \in X_{\mathrm{H},h} \times X_{\mathrm{H},h} \times \big(X_{\mathrm{H},h} \cap L^2_0(\Omega_{\mathrm{H}})\big) \times X_{\mathrm{T},h}$ with $\zeta = \psi$ on Σ. Equivalently, using (4.34), the heart-torso subproblem (4.38) can be split into two coupled, torso (Dirichlet) and heart (Neumann), subproblems as follows:

- Find $u_{\mathrm{T}}^{n+1} \in X_{\mathrm{T},h}$, with $u_{\mathrm{T}}^{n+1} = u_{\mathrm{e}}^{n+1}$ on Σ, such that

$$\int_{\Omega_{\mathrm{T}}} \boldsymbol{\sigma}_{\mathrm{T}} \boldsymbol{\nabla} u_{\mathrm{T}}^{n+1} \cdot \boldsymbol{\nabla} \zeta = 0 \tag{4.39}$$

  for all $\zeta \in X_{\mathrm{T},h}$, with $\zeta = 0$ on Σ.

- Find $u_{\mathrm{e}}^{n+1} \in X_{\mathrm{H},h} \cap L^2_0(\Omega_{\mathrm{H}})$ such that

$$\int_{\Omega_{\mathrm{H}}} (\boldsymbol{\sigma}_{\mathrm{i}} + \boldsymbol{\sigma}_{\mathrm{e}}) \boldsymbol{\nabla} u_{\mathrm{e}}^{n+1} \cdot \boldsymbol{\nabla} \psi + \int_{\Omega_{\mathrm{H}}} \boldsymbol{\sigma}_{\mathrm{i}} \boldsymbol{\nabla} V_{\mathrm{m}}^{\star} \cdot \boldsymbol{\nabla} \psi = - \int_{\Omega_{\mathrm{T}}} \boldsymbol{\sigma}_{\mathrm{T}} \boldsymbol{\nabla} u_{\mathrm{T}}^{n+1} \cdot \boldsymbol{\nabla} \mathcal{L}_h \psi \tag{4.40}$$

  for all $\psi \in X_{\mathrm{H},h} \cap L^2_0(\Omega_{\mathrm{H}})$.

Remark 4.1 *The residual term in the right hand side of* (4.40) *amounts to enforce the Neumann condition* (2.15) *in a variational consistent fashion.*

Despite the Gauss-Seidel and Jacobi splittings allow a decoupled solution of (4.36) and (4.37), the heart and torso potentials u_{e}^{n+1} and u_{T}^{n+1} are still implicitly coupled. Therefore, problems (4.39) and (4.40) must be solved simultaneously: either *monolithically*, after assembling of (4.38) (see *e.g.* [43, 30, 44, 48]) or, in a *partitioned* fashion, by sub-iterating between them (see *e.g.* [9, 4]). Note that, since the (quasi-static) time discretizations (4.39) and (4.40) do not generate numerical dissipation in time, the naive Dirichlet-Neumann explicit coupling, obtained by enforcing

$$u_{\mathrm{T}}^{n+1} = u_{\mathrm{e}}^{n} \quad \text{on} \quad \Sigma,$$

in the torso subproblem (4.39), might lead to numerical instability.

In the next subsection, we introduce an alternative heart-torso splitting, based on Robin-Robin transmission conditions, which remains stable under a mild CFL like condition.

4.2 Fully discrete formulation: decoupled time-marching schemes

We propose to combine the decoupling techniques introduced in section §3 with the following explicit Robin-Robin splitting, derived from [1] (see also [10]), of the heart-torso coupling:

$$\begin{aligned}
\boldsymbol{\sigma}_{\mathrm{e}} \boldsymbol{\nabla} u_{\mathrm{e}}^{n+1} \cdot \boldsymbol{n} + \frac{\gamma \sigma_{\mathrm{T}}^{\mathrm{t}}}{h} u_{\mathrm{e}}^{n+1} &= -\boldsymbol{\sigma}_{\mathrm{T}} \boldsymbol{\nabla} u_{\mathrm{T}}^{n} \cdot \boldsymbol{n}_{\mathrm{T}} + \frac{\gamma \sigma_{\mathrm{T}}^{\mathrm{t}}}{h} u_{\mathrm{T}}^{n}, \quad \text{on} \quad \Sigma, \\
\boldsymbol{\sigma}_{\mathrm{T}} \boldsymbol{\nabla} u_{\mathrm{T}}^{n+1} \cdot \boldsymbol{n}_{\mathrm{T}} + \frac{\gamma \sigma_{\mathrm{T}}^{\mathrm{t}}}{h} u_{\mathrm{T}}^{n+1} &= \boldsymbol{\sigma}_{\mathrm{T}} \boldsymbol{\nabla} u_{\mathrm{T}}^{n} \cdot \boldsymbol{n}_{\mathrm{T}} + \frac{\gamma \sigma_{\mathrm{T}}^{\mathrm{t}}}{h} u_{\mathrm{e}}^{n+1}, \quad \text{on} \quad \Sigma,
\end{aligned} \tag{4.41}$$

where $\gamma > 0$ is a free Robin parameter, to be specified later on, and $\sigma_{\mathrm{T}}^{\mathrm{t}}$ is such that $\boldsymbol{\sigma}_{\mathrm{T}|\Sigma} = \sigma_{\mathrm{T}}^{\mathrm{t}} \boldsymbol{I}$.

Remark 4.2 *We have assumed, without loss of generality, that the torso conductivity tensor is isotropic on the boundary, $\boldsymbol{\sigma}_{\mathrm{T}|\Sigma} = \sigma_{\mathrm{T}}^{\mathrm{t}}\boldsymbol{I}$, and that $\sigma_{\mathrm{T}}^{\mathrm{t}}$ is constant.*

Thus, the resulting schemes read as follows: for $0 \le n \le N-1$, we solve:

1. Ionic state: find $w^{n+1} \in X_h$ such that

$$\int_{\Omega_{\mathrm{H}}} \left(D_\tau w^{n+1} + g(V_{\mathrm{m}}^n, w^{n+1})\right)\xi = 0 \tag{4.42}$$

   for all $\xi \in X_h$.

2. Transmembrane potential: find $V_{\mathrm{m}}^{n+1} \in X_h$ such that

$$\chi_{\mathrm{m}} \int_{\Omega_{\mathrm{H}}} D_\tau V_{\mathrm{m}}^{n+1}\phi + \int_{\Omega_{\mathrm{H}}} \boldsymbol{\sigma}_{\mathrm{i}}\boldsymbol{\nabla} V_{\mathrm{m}}^{n+1}\cdot\boldsymbol{\nabla}\phi + \int_{\Omega_{\mathrm{H}}} \boldsymbol{\sigma}_{\mathrm{i}}\boldsymbol{\nabla} u_{\mathrm{e}}^{\star}\cdot\boldsymbol{\nabla}\phi = \int_{\Omega_{\mathrm{H}}} \left(I_{\mathrm{app}}^{n+1} - I_{\mathrm{ion}}(V_{\mathrm{m}}^n, w^{n+1})\right)\phi \tag{4.43}$$

   for all $\phi \in X_h$.

3. Extracellular potential: find $u_{\mathrm{e}}^{n+1} \in X_h$ such that

$$\int_{\Omega_{\mathrm{H}}} (\boldsymbol{\sigma}_{\mathrm{i}} + \boldsymbol{\sigma}_{\mathrm{e}})\boldsymbol{\nabla} u_{\mathrm{e}}^{n+1}\cdot\boldsymbol{\nabla}\psi + \int_{\Omega_{\mathrm{H}}} \boldsymbol{\sigma}_{\mathrm{i}}\boldsymbol{\nabla} V_{\mathrm{m}}^{\star}\cdot\boldsymbol{\nabla}\psi + \frac{\gamma\sigma_{\mathrm{T}}^{\mathrm{t}}}{h}\int_{\Sigma} u_{\mathrm{e}}^{n+1}\psi = -\int_{\Sigma} \boldsymbol{\sigma}_{\mathrm{T}}\boldsymbol{\nabla} u_{\mathrm{T}}^{n}\cdot\boldsymbol{n}_{\mathrm{T}}\psi + \frac{\gamma\sigma_{\mathrm{T}}^{\mathrm{t}}}{h}\int_{\Sigma} u_{\mathrm{T}}^{n}\psi \tag{4.44}$$

   for all $\psi \in X_h$.

4. Torso potential: find $u_{\mathrm{T}}^{n+1} \in X_h$

$$\int_{\Omega_{\mathrm{T}}} \boldsymbol{\sigma}_{\mathrm{T}}\boldsymbol{\nabla} u_{\mathrm{T}}^{n+1}\cdot\boldsymbol{\nabla}\zeta + \frac{\gamma\sigma_{\mathrm{T}}^{\mathrm{t}}}{h}\int_{\Sigma} u_{\mathrm{T}}^{n+1}\zeta = \int_{\Sigma} \boldsymbol{\sigma}_{\mathrm{T}}\boldsymbol{\nabla} u_{\mathrm{T}}^{n}\cdot\boldsymbol{n}_{\mathrm{T}}\zeta + \frac{\gamma\sigma_{\mathrm{T}}^{\mathrm{t}}}{h}\int_{\Sigma} u_{\mathrm{e}}^{n+1}\zeta \tag{4.45}$$

   for all $\zeta \in X_h$.

Contrarily to (4.36)-(4.38), the cardiac subproblem (4.42)-(4.44) can be solved independently of the torso subproblem (4.45). In particular, the choices $(u_{\mathrm{e}}^{\star}, V_{\mathrm{m}}^{\star}) = (u_{\mathrm{e}}^{n}, V_{\mathrm{m}}^{n+1})$ or $(u_{\mathrm{e}}^{\star}, V_{\mathrm{m}}^{\star}) = (u_{\mathrm{e}}^{n}, V_{\mathrm{m}}^{n})$ lead to a fully decoupled computation of w^{n+1}, V_{m}^{n+1}, u_{e}^{n+1} and u_{T}^{n+1}. In other words, the four subproblems (4.42)-(4.45) are decoupled and can be solved sequentially.

The energy based numerical stability of these schemes is addressed in the next subsection.

Remark 4.3 *The choices $(u_{\mathrm{e}}^{\star}, V_{\mathrm{m}}^{\star}) = (u_{\mathrm{e}}^{n}, V_{\mathrm{m}}^{n+1})$ or $(u_{\mathrm{e}}^{\star}, V_{\mathrm{m}}^{\star}) = (u_{\mathrm{e}}^{n}, V_{\mathrm{m}}^{n})$ in (4.42)-(4.45) allow a fully decoupled computation of w^{n+1}, V_{m}^{n+1}, u_{e}^{n+1} and u_{T}^{n+1} without the need to resort to monodomain and uncoupling approximations (see Remark 2.3).*

4.3 Stability analysis

We address here the energy based stability of the heart-torso coupling schemes (4.42)-(4.45). Hence, in order to alleviate the exposition, we denote by $E_{\mathrm{H}}^0(u_{\mathrm{e}}^\star, V_{\mathrm{m}}^\star)$ (resp. $E_{\mathrm{H}}^n(u_{\mathrm{e}}^\star, V_{\mathrm{m}}^\star)$) the discrete bidomain energy at steps 0 (resp. n), arising in the stability estimates provided by Theorem 3.2. For instance, in the case $(u_{\mathrm{e}}^\star, V_{\mathrm{m}}^\star) = (u_{\mathrm{e}}^n, V_{\mathrm{m}}^n)$, we have

$$
\begin{aligned}
E_{\mathrm{H}}^0(u_{\mathrm{e}}^\star, V_{\mathrm{m}}^\star) &\stackrel{\mathrm{def}}{=} \|w^0\|_{0,\Omega_{\mathrm{H}}}^2 + \chi_{\mathrm{m}}\|V_{\mathrm{m}}^0\|_{0,\Omega_{\mathrm{H}}}^2 + \tau\|\boldsymbol{\sigma}_{\mathrm{i}}^{\frac{1}{2}}\boldsymbol{\nabla} V_{\mathrm{m}}^0\|_{0,\Omega_{\mathrm{H}}}^2 + \tau\|\boldsymbol{\sigma}_{\mathrm{i}}^{\frac{1}{2}}\boldsymbol{\nabla} u_{\mathrm{e}}^0\|_{0,\Omega_{\mathrm{H}}}^2,\\
E_{\mathrm{H}}^n(u_{\mathrm{e}}^\star, V_{\mathrm{m}}^\star) &\stackrel{\mathrm{def}}{=} \|w^n\|_{0,\Omega_{\mathrm{H}}}^2 + \chi_{\mathrm{m}}\|V_{\mathrm{m}}^n\|_{0,\Omega_{\mathrm{H}}}^2 + \tau\|\boldsymbol{\sigma}_{\mathrm{i}}^{\frac{1}{2}}\boldsymbol{\nabla} u_{\mathrm{e}}^n\|_{0,\Omega_{\mathrm{H}}}^2 + \tau\|\boldsymbol{\sigma}_{\mathrm{i}}^{\frac{1}{2}}\boldsymbol{\nabla} V_{\mathrm{m}}^n\|_{0,\Omega_{\mathrm{H}}}^2\\
&\quad + 2\sum_{m=0}^{n-1}\tau\|\boldsymbol{\sigma}_{\mathrm{e}}^{\frac{1}{2}}\boldsymbol{\nabla} u_{\mathrm{e}}^{m+1}\|_{0,\Omega_{\mathrm{H}}}^2,
\end{aligned}
$$

and similarly for the rest.

The next theorem states the main result of this section.

Theorem 4.4 *Assume that the hypothesis of Theorem 3.2 hold and that the torso conductivity tensor $\boldsymbol{\sigma}_{\mathrm{T}}$ is symmetric and positive-definite. Let $\{(w^n, V_{\mathrm{m}}^n, u_{\mathrm{e}}^n, u_{\mathrm{T}}^n)\}_{n=0}^N$ be solution of* (4.42)-(4.45)*. Then for*

$$
\gamma > 2C_{\mathrm{ti}}, \tag{4.46}
$$

the following estimate holds

$$
\begin{aligned}
&E_{\mathrm{H}}^n(u_{\mathrm{e}}^\star, V_{\mathrm{m}}^\star) + \tau\frac{\gamma\sigma_{\mathrm{T}}^{\mathrm{t}}}{h}\|u_{\mathrm{T}}^n\|_{0,\Sigma}^2 + \sum_{m=0}^{n-1}\tau\|\boldsymbol{\sigma}_{\mathrm{T}}^{\frac{1}{2}}\boldsymbol{\nabla} u_{\mathrm{T}}^{m+1}\|_{0,\Omega_{\mathrm{T}}}^2 + \sum_{m=0}^{n-1}\tau\frac{\gamma\sigma_{\mathrm{T}}^{\mathrm{t}}}{2h}\|u_{\mathrm{T}}^{m+1} - u_{\mathrm{e}}^{m+1}\|_{0,\Sigma}^2\\
&\leq C(T,\alpha,\beta)\left(E_{\mathrm{H}}^0(u_{\mathrm{e}}^\star, V_{\mathrm{m}}^\star) + \tau\frac{\gamma\sigma_{\mathrm{T}}^{\mathrm{t}}}{h}\|u_{\mathrm{T}}^0\|_{0,\Sigma}^2 + \tau\|\boldsymbol{\sigma}_{\mathrm{T}}^{\frac{1}{2}}\boldsymbol{\nabla} u_{\mathrm{T}}^0\|_{0,\Omega_{\mathrm{T}}}^2 + \sum_{m=0}^{n-1}\tau\|I_{\mathrm{app}}^{m+1}\|_{0,\Omega_{\mathrm{H}}}^2\right),
\end{aligned}
\tag{4.47}
$$

with $1 \leq n \leq N$. In particular, (4.47) *ensures the energy based stability of the explicit heart-torso coupling* (4.42)-(4.45) *under the condition $\tau = O(h)$.*

Proof. Since the stability of the heart-torso coupling (4.44)-(4.45) does not depend on the choice of $u_{\mathrm{e}}^\star$ and $V_{\mathrm{m}}^\star$, we restrict ourselves to the case $(u_{\mathrm{e}}^\star, V_{\mathrm{m}}^\star) = (u_{\mathrm{e}}^n, V_{\mathrm{m}}^n)$. The rest of estimates can be derived in a similar fashion.

By testing (3.20)-(3.22) with $(\xi,\phi,\psi,\zeta) = \tau(w^{n+1}, V_{\mathrm{m}}^{n+1}, u_{\mathrm{e}}^{n+1}, u_{\mathrm{T}}^{n+1})$ and after summation of the resulting expressions we have:

$$
\begin{aligned}
&\frac{1}{2}\left(\|w^{n+1}\|_{0,\Omega_{\mathrm{H}}}^2 - \|w^n\|_{0,\Omega_{\mathrm{H}}}^2\right) + \frac{\chi_{\mathrm{m}}}{2}\left(\|V_{\mathrm{m}}^{n+1}\|_{0,\Omega_{\mathrm{H}}}^2 - \|V_{\mathrm{m}}^n\|_{0,\Omega_{\mathrm{H}}}^2\right) + \tau\|\boldsymbol{\sigma}_{\mathrm{e}}^{\frac{1}{2}}\boldsymbol{\nabla} u_{\mathrm{e}}^{n+1}\|_{0,\Omega_{\mathrm{H}}}^2\\
&+ \tau\|\boldsymbol{\sigma}_{\mathrm{i}}^{\frac{1}{2}}\boldsymbol{\nabla}(V_{\mathrm{m}}^{n+1} + u_{\mathrm{e}}^{n+1})\|_{0,\Omega_{\mathrm{H}}}^2 + \tau\|\boldsymbol{\sigma}_{\mathrm{T}}^{\frac{1}{2}}\boldsymbol{\nabla} u_{\mathrm{T}}^{n+1}\|_{0,\Omega_{\mathrm{T}}}^2 + \frac{\tau\gamma\sigma_{\mathrm{T}}^{\mathrm{t}}}{h}\|u_{\mathrm{T}}^{n+1} - u_{\mathrm{e}}^{n+1}\|_{0,\Sigma}^2\\
&\underbrace{+\frac{\tau\gamma\sigma_{\mathrm{T}}^{\mathrm{t}}}{h}\int_\Sigma (u_{\mathrm{T}}^{n+1} - u_{\mathrm{T}}^n)u_{\mathrm{e}}^{n+1}}_{I_4} \underbrace{-\tau\int_\Sigma \boldsymbol{\sigma}_{\mathrm{T}}\boldsymbol{\nabla} u_{\mathrm{T}}^n\cdot\boldsymbol{n}_{\mathrm{T}}(u_{\mathrm{T}}^{n+1} - u_{\mathrm{e}}^{n+1})}_{I_5} + I_1 + I_3 \leq I_2.
\end{aligned}
\tag{4.48}
$$

Terms I_1, I_2 and I_3 have already been estimated in the proof of Theorem 3.2, so we only need to provide bounds for I_4 and I_5.

Term I_4 is treated as follows (see [1, 10]),

$$\begin{aligned} I_4 =& \frac{\tau\gamma\sigma_{\mathrm{T}}^{\mathrm{t}}}{h}\int_\Sigma \big(u_{\mathrm{T}}^{n+1}-u_{\mathrm{T}}^{n}\big)\big(u_{\mathrm{e}}^{n+1}-u_{\mathrm{T}}^{n+1}\big)+\frac{\tau\gamma\sigma_{\mathrm{T}}^{\mathrm{t}}}{h}\int_\Sigma \big(u_{\mathrm{T}}^{n+1}-u_{\mathrm{T}}^{n}\big)u_{\mathrm{T}}^{n+1} \\ \geq& -\frac{\tau\gamma\sigma_{\mathrm{T}}^{\mathrm{t}}}{2h}\big\|u_{\mathrm{T}}^{n+1}-u_{\mathrm{T}}^{n}\big\|_{0,\Sigma}^2-\frac{\tau\gamma\sigma_{\mathrm{T}}^{\mathrm{t}}}{2h}\big\|u_{\mathrm{e}}^{n+1}-u_{\mathrm{T}}^{n+1}\big\|_{0,\Sigma}^2 \\ &+\frac{\tau\gamma\sigma_{\mathrm{T}}^{\mathrm{t}}}{2h}\Big(\big\|u_{\mathrm{T}}^{n+1}\big\|_{0,\Sigma}^2-\big\|u_{\mathrm{T}}^{n}\big\|_{0,\Sigma}^2\Big)+\frac{\tau\gamma\sigma_{\mathrm{T}}^{\mathrm{t}}}{2h}\big\|u_{\mathrm{T}}^{n+1}-u_{\mathrm{T}}^{n}\big\|_{0,\Sigma}^2 \\ =& \frac{\tau\gamma\sigma_{\mathrm{T}}^{\mathrm{t}}}{2h}\Big(\big\|u_{\mathrm{T}}^{n+1}\big\|_{0,\Sigma}^2-\big\|u_{\mathrm{T}}^{n}\big\|_{0,\Sigma}^2\Big)-\frac{\tau\gamma\sigma_{\mathrm{T}}^{\mathrm{t}}}{2h}\big\|u_{\mathrm{e}}^{n+1}-u_{\mathrm{T}}^{n+1}\big\|_{0,\Sigma}^2. \end{aligned} \tag{4.49}$$

On the other hand, using (4.35), for the last term we have

$$\begin{aligned} I_5 \geq& -\frac{\tau h}{\gamma}\big\|(\sigma_{\mathrm{T}}^{\mathrm{t}})^{\frac12}\boldsymbol{\nabla} u_{\mathrm{T}}^{n}\big\|_{0,\Sigma}^2-\frac{\tau\gamma\sigma_{\mathrm{T}}^{\mathrm{t}}}{4h}\big\|u_{\mathrm{e}}^{n+1}-u_{\mathrm{T}}^{n+1}\big\|_{0,\Sigma}^2 \\ \geq& -\frac{\tau C_{\mathrm{ti}}}{\gamma}\big\|\boldsymbol{\sigma}_{\mathrm{T}}^{\frac12}\boldsymbol{\nabla} u_{\mathrm{T}}^{n}\big\|_{0,\Omega_{\mathrm{T}}}^2-\frac{\tau\gamma\sigma_{\mathrm{T}}^{\mathrm{t}}}{4h}\big\|u_{\mathrm{e}}^{n+1}-u_{\mathrm{T}}^{n+1}\big\|_{0,\Sigma}^2. \end{aligned} \tag{4.50}$$

Therefore, by inserting (3.29), (3.30), (3.32), (4.49) and (4.50) into (4.48) we get the estimate

$$\begin{aligned} &\frac12\left(\|w^{n+1}\|_{0,\Omega_{\mathrm{H}}}^2-\|w^{n}\|_{0,\Omega_{\mathrm{H}}}^2\right)+\frac{\chi_{\mathrm{m}}}{2}\left(\|V_{\mathrm{m}}^{n+1}\|_{0,\Omega_{\mathrm{H}}}^2-\|V_{\mathrm{m}}^{n}\|_{0,\Omega_{\mathrm{H}}}^2\right) \\ &\quad+\tau\|\boldsymbol{\sigma}_{\mathrm{e}}^{\frac12}\boldsymbol{\nabla} u_{\mathrm{e}}^{n+1}\|_{0,\Omega_{\mathrm{H}}}^2+\tau\left(\big\|\boldsymbol{\sigma}_{\mathrm{T}}^{\frac12}\boldsymbol{\nabla} u_{\mathrm{T}}^{n+1}\big\|_{0,\Omega_{\mathrm{T}}}^2-\frac{C_{\mathrm{ti}}}{\gamma}\big\|\boldsymbol{\sigma}_{\mathrm{T}}^{\frac12}\boldsymbol{\nabla} u_{\mathrm{T}}^{n}\big\|_{0,\Omega_{\mathrm{T}}}^2\right) \\ &\quad+\frac{\tau\gamma\sigma_{\mathrm{T}}^{\mathrm{t}}}{4h}\big\|u_{\mathrm{T}}^{n+1}-u_{\mathrm{e}}^{n+1}\big\|_{0,\Sigma}^2+\frac{\tau\gamma\sigma_{\mathrm{T}}^{\mathrm{t}}}{2h}\Big(\big\|u_{\mathrm{T}}^{n+1}\big\|_{0,\Sigma}^2-\big\|u_{\mathrm{T}}^{n}\big\|_{0,\Sigma}^2\Big) \\ &\quad+\frac{\tau}{2}\left(\|\boldsymbol{\sigma}_{\mathrm{i}}^{\frac12}\boldsymbol{\nabla} V_{\mathrm{m}}^{n+1}\|_{0,\Omega_{\mathrm{H}}}^2-\|\boldsymbol{\sigma}_{\mathrm{i}}^{\frac12}\boldsymbol{\nabla} V_{\mathrm{m}}^{n}\|_{0,\Omega_{\mathrm{H}}}^2\right) \\ &\quad+\frac{\tau}{2}\left(\|\boldsymbol{\sigma}_{\mathrm{i}}^{\frac12}\boldsymbol{\nabla} u_{\mathrm{e}}^{n+1}\|_{0,\Omega_{\mathrm{H}}}^2-\|\boldsymbol{\sigma}_{\mathrm{i}}^{\frac12}\boldsymbol{\nabla} u_{\mathrm{e}}^{n}\|_{0,\Omega_{\mathrm{H}}}^2\right) \\ &\quad\leq\frac{\tau}{2}\|I_{\mathrm{app}}^{n+1}\|_{0,\Omega_{\mathrm{H}}}^2+\frac{\tau\alpha}{2}\|V_{\mathrm{m}}^{n+1}\|_{0,\Omega_{\mathrm{H}}}^2+\frac{\tau\beta}{2}\|w^{n+1}\|_{0,\Omega_{\mathrm{H}}}^2. \end{aligned}$$

Estimate (4.47) then follows, under conditions (4.46) and (3.24), by replacing index n by m, summing over $0\leq m\leq n-1$ and applying Gronwall's lemma, which completes the proof.

Remark 4.5 *The above proof does not make use of any numerical dissipation apart from that directly provided by the explicit Robin-Robin splitting* (4.41)*. Note that this is particularly well adapted to the heart-torso coupling* (2.8)-(2.16)*, since the quasi-static elliptic equations* (2.9) *and* (2.10) *do not generate numerical dissipation in time.*

Remark 4.6 *The flux terms in* (4.44) *and* (4.45) *can be evaluated face-wise, i.e. as broken integrals, or using a discrete variational expression, as in* (4.40)*. Hence,* $\int_\Sigma \boldsymbol{\sigma}_{\mathrm{T}}\boldsymbol{\nabla} u_{\mathrm{T}}^n\cdot\boldsymbol{n}_{\mathrm{T}}\psi$ *and* $\int_\Sigma \boldsymbol{\sigma}_{\mathrm{T}}\boldsymbol{\nabla} u_{\mathrm{T}}^n\cdot\boldsymbol{n}_{\mathrm{T}}\zeta$*, can be safely replaced by* $\int_{\Omega_{\mathrm{T}}}\boldsymbol{\sigma}_{\mathrm{T}}\boldsymbol{\nabla} u_{\mathrm{T}}^n\cdot\boldsymbol{\nabla}\mathcal{L}_h\psi$ *and* $\int_{\Omega_{\mathrm{T}}}\boldsymbol{\sigma}_{\mathrm{T}}\boldsymbol{\nabla} u_{\mathrm{T}}^n\cdot\boldsymbol{\nabla}\mathcal{L}_h\zeta$*, respectively.*

5 Numerical results

In this section we illustrate, via numerical simulations based on anatomical heart and torso geometries, the stability and accuracy of the explicit splitting schemes analyzed in the previous sections. Numerical results for an isolated bidomain model using the time-marching procedures of section §3 are presented in subsection §5.2. Subsection §5.3 demonstrates the capabilities of the splitting schemes introduced in section §4 to provide accurate 12-lead ECG signals.

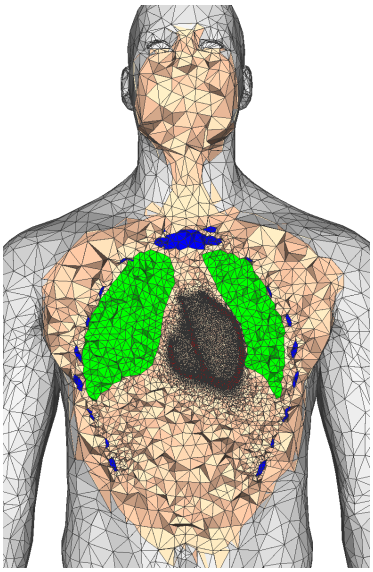

Figure 2: Cut view of the heart-torso computational mesh: heart (red) lungs (green), bone (blue) and remaining tissue (apricot).

5.1 Simulation data

The simulations are performed with the anatomical data and the model parameters used in [11, 12]. For the sake of conciseness we only report here the main ingredients (full details are given in [11, 12]).

The computational heart and torso meshes were obtained starting from the Zygote (`www.3dscience.com`) anatomical model, using the `3-matic` software (`www.materialise.com`) to obtain computationally-correct surface meshes. The mesh, displayed in Figure 2, contains the heart, lung, bones and remaining extramyocardial tissue. They have been obtained by processing the surface meshes with `Yams` [20] and `GHS3D` [21]. The volume heart and torso meshes are made of 542 000 and 1 242 000 tetrahedra, respetively.

The bidomain model parameters are given in Table 1, where $\sigma_{\mathrm{i,e}}^{\mathrm{l}}$ (resp. $\sigma_{\mathrm{i,e}}^{\mathrm{t}}$) denotes the scalar intra- and extracelluar longitudinal (resp. transverse) conductivities. Table 2 provides the conductivity parameters for the torso (supposed isotropic).

As in [4], a rescaled version of the two-variable model proposed by Mitchell and Schaeffer in [32] is considered as ionic model. Functions g and I_{ion} are then

A_m (cm^{-1})	C_m (mF)	σ_i^l (S cm^{-1})	σ_e^l (S cm^{-1})	σ_i^t (S cm^{-1})	σ_e^t (S cm^{-1})
500	10^{-3}	3.0×10^{-3}	3.0×10^{-3}	3.0×10^{-4}	1.2×10^{-3}

Table 1: Bidomain model parameters.

σ_T^t (S cm^{-1})	σ_T^l (S cm^{-1})	σ_T^b (S cm^{-1})
6.0×10^{-4}	2.4×10^{-4}	4.0×10^{-5}

Table 2: Torso conductivity parameters: tissue (t), lungs (l) and bone (b).

given by

$$I_{ion}(V_m, w) = -w\frac{(V_m - V_{min})^2(V_{max} - V_m)}{\tau_{in}(V_{max} - V_{min})} + \frac{V_m - V_{min}}{\tau_{out}(V_{max} - V_{min})},$$

$$g(V_m, w) = \begin{cases} \dfrac{w}{\tau_{open}} - \dfrac{1}{\tau_{open}(V_{max} - V_{min})^2} & \text{if} \quad V_m < V_{gate}, \\ \dfrac{w}{\tau_{close}} & \text{if} \quad V_m \geq V_{gate}, \end{cases}$$

where the values of the free parameters τ_{in}, τ_{out}, τ_{open}, τ_{close}, V_{gate} are reported in Table 3, and V_{min}, V_{max} are scaling constants (-80 and 20 mV, respectively).

τ_{in}	τ_{out}	τ_{open}	τ_{close}^{RV}	$\tau_{close}^{LV-endo}$	τ_{close}^{LV-epi}	V_{gate}
4.5	90	100	120	140	105	-67

Table 3: Mitchell-Schaeffer ionic model parameters.

Continuous $\mathbb{P}_1$ Lagrange finite elements are used forthe space discretization of both the heart and the torso equations. The time step size was fixed to $\tau = 0.25$ ms and the Robin parameter, for the heart-torso coupling scheme (4.42)-(4.45), to $\gamma = 0.1$.

5.2 Isolated heart

The isolated bidomain equations (3.20)-(3.22) are approximated using the time-marching schemes (3.21)-(3.22). In what follows, we shall refer to each of these schemes using the following terminology:

- *Coupled*: $(u_e^\star, V_m^\star) = (u_e^{n+1}, V_m^{n+1})$;
- *Gauss-Seidel*: $(u_e^\star, V_m^\star) = (u_e^n, V_m^{n+1})$;
- *Jacobi*: $(u_e^\star, V_m^\star) = (u_e^n, V_m^n)$.

The time course of the transmembrane and extracellular potentials at a given epicardial location are displayed in Figure 3. We can observe that the simulations are numerically stable and the curves are practically indistinguishable. Somehow, this is not surprising since the electrodiffusive Gauss-Seidel and Jacobi splittings are expected to still provide optimal first order accuracy. A slight difference can be seen after axis rescaling, as shown in Figure 4.

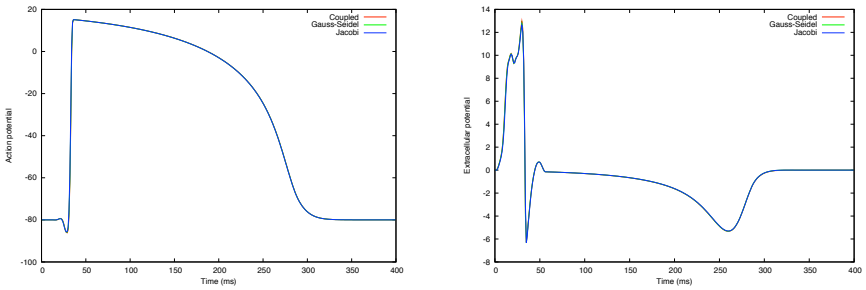

Figure 3: Time course of the transmembrane potential (left) and extracellular potential (right) at a given location in the epicardium.

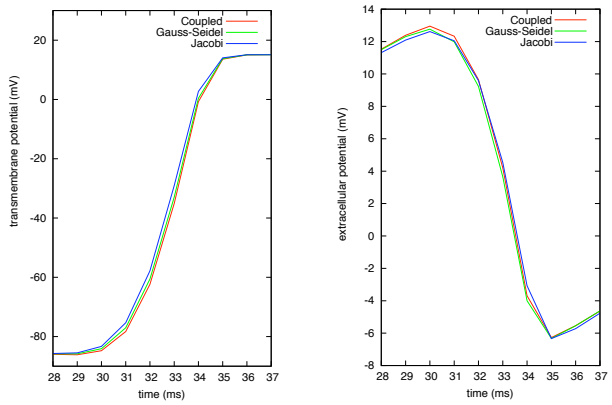

Figure 4: Time course, after axis rescaling, of the transmembrane potential (left) and extracellular potential (right) at a given location in the epicardium.

scheme / τ (ms)	Coupled	Gauss-Seidel	Jacobi
0.25	✓	✓	✓
0.50	✓	✓	✓
1.00	✓	✓	✓
1.25	✗	✗	✗
1.50	✗	✗	✗

Table 4: Stability sensitivity to the time step size τ. Symbol ✗ indicates numerical instability.

The results reported in Table 4 confirm that the electrodiffusive Gauss-Seidel and Jacobi splittings do not introduce additional constraints on the time step size τ, as predicted by Theorem 3.2.

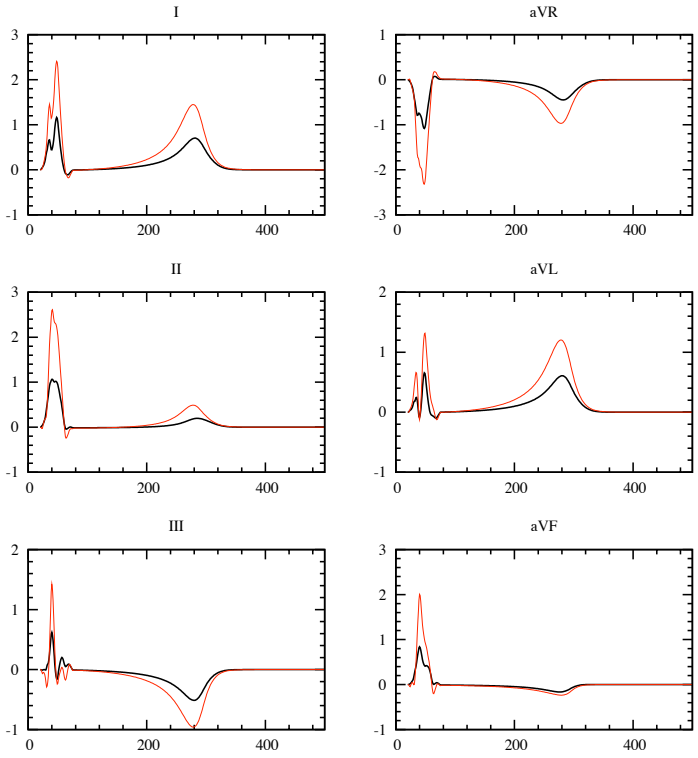

Figure 5: Simulated ECG signals (standard and augmented leads) obtained using heart-torso full coupling (balck) and uncoupling (red).

5.3 12-lead ECG

For comparison purposes, the simulated 12-lead ECG signals obtained with the explicit coupling procedures (3.21)-(3.22) will be compared with those obtained using heart-torso coupling (see *e.g.* [29, 4]) and heart-torso uncoupling (see *e.g.* [4]). We shall refer to each of the considered schemes according to the following terminology:

- *Full coupling*: $(u_{\rm e}^\star, V_{\rm m}^\star) = (u_{\rm e}^{n+1}, V_{\rm m}^{n+1})$ in (4.36)-(4.38);
- *Uncoupling*: $(u_{\rm e}^\star, V_{\rm m}^\star) = (u_{\rm e}^{n+1}, V_{\rm m}^{n+1})$ and heart-torso uncoupling (see Remark 2.2 and *e.g.* [4]).
- *Robin*: $(u_{\rm e}^\star, V_{\rm m}^\star, u_{\rm T}^\star) = (u_{\rm e}^{n+1}, V_{\rm m}^{n+1}, u_{\rm T}^n)$ in (4.42)-(4.45);
- *Gauss-Seidel-Robin*: $(u_{\rm e}^\star, V_{\rm m}^\star, u_{\rm T}^\star) = (u_{\rm e}^n, V_{\rm m}^{n+1}, u_{\rm T}^n)$ in (4.42)-(4.45);
- *Jacobi-Robin*: $(u_{\rm e}^\star, V_{\rm m}^\star, u_{\rm T}^\star) = (u_{\rm e}^n, V_{\rm m}^n, u_{\rm T}^n)$ in (4.42)-(4.45);

In Figures 5 and 6 we provide the complete 12-lead ECG signals obtained using the full coupling (black) and uncoupling (red) approaches. We can observe that the uncoupling approach is unable to reproduce the correct signal amplitude, which is indeed magnified by a factor close to 2 in practically all the

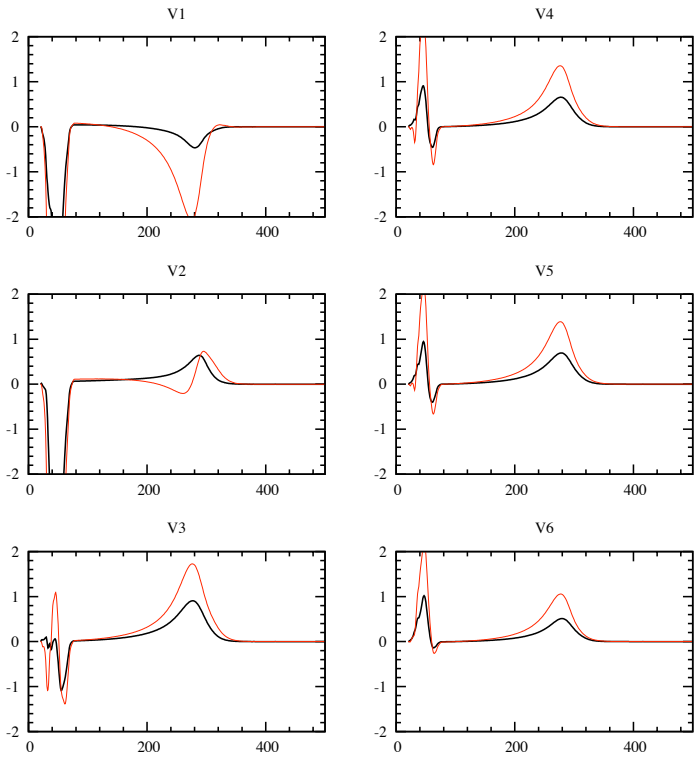

Figure 6: Simulated ECG signals (chest leads) obtained using heart-torso full coupling (balck) and uncoupling (red).

ECG leads. Moreover, the shape mismatch in some of the leads is clearly visible: the QRS complex in V3 and the T-wave in V2, for instance. Similar observations have been reported in [4] (see also [29]), for both healthy and pathological conditions.

In the next paragraphs, we shall see that (for an equivalent computational cost) the Robin based explicit coupling introduced in section §4 provides much more accurate ECG signals. For illustration purposes, in Figure 10, we have reported some snapshots of the body surface potentials obtained with the Jacobi-Robin scheme. Figure 9 shows a posterior view of the potential within the torso and the heart. The potential matching at the heart-torso interface is clearly visible.

In Figures 7 and 8 we compare the simulated 12-lead ECG signals obtained with full coupling (black) to those obtained with fully decoupled Jacobi-Robin scheme (red). The improved accuracy with respect to the uncoupling approach is striking. Indeed, the signals are practically indistinguishable in all the 12 leads. Some minor differences are visible in the QRS complex of V2 and V3. Similar results are obtained with the Robin and Gauss-Seidel-Robin schemes, that we omit for the sake of conciseness. Nevertheless, in order to illustrate the impact of the level of decoupling in the accuracy of the ECG, we have reported in Figure 11 a rescaled comparison of the QRS complex (left) and T-wave (right) of

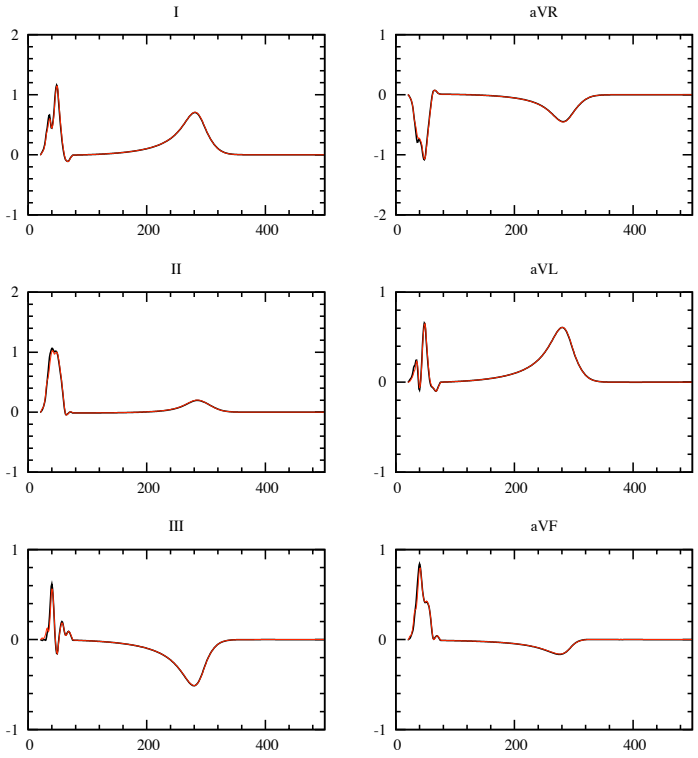

Figure 7: Simulated ECG signals (standard and augmented leads) obtained using heart-torso full coupling (balck) and the Jacobi-Robin scheme (red).

the first ECG lead, obtained with the full coupling, Robin, Gauss-Seidel-Robin and Jacobin-Robin approaches. No significant differences are observed in the T-wave, whereas slightly better results are obtained with the Robin approach in the QRS-complex.

The 12-lead ECG signals of a pathological situation, a left bundle branch block (LBBB), have been also computed to illustrate the robustness of the proposed splitting schemes. Figures 12 and 13 presents the corresponding signals obtained with the full coupling (black) and Jacobi-Robin (red) schemes. Once more, the decoupled scheme shows very good accuracy and stability.

Finally, we go further in the investigation of the robustness of the schemes, by considering different heart and torso geometries and model parameters. In particular, we keep $\gamma = 0.1$ as in the previous cases. To this aim, we revisit the ECG numerical simulations recently reported in [4]. Figures 14 and 15 the corresponding signals obtained with the full coupling (black) and Jacobi-Robin (red) schemes. Once more, both signals are in excellent agreement. Similar results have been obtained for a LBBB pathology, that we omit here for the sake of conciseness.

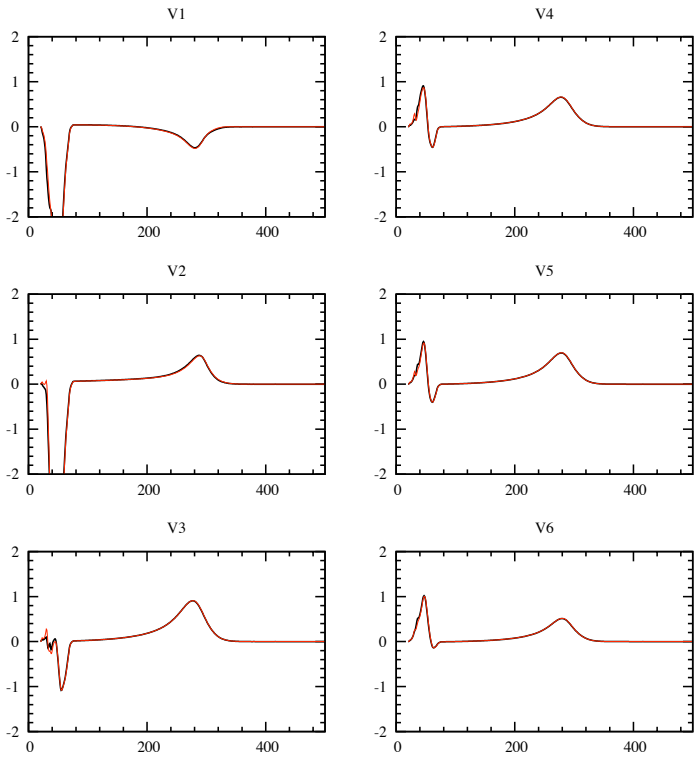

Figure 8: Simulated ECG signals (chest leads) obtained using heart-torso full coupling (balck) and the Jacobi-Robin scheme (red).

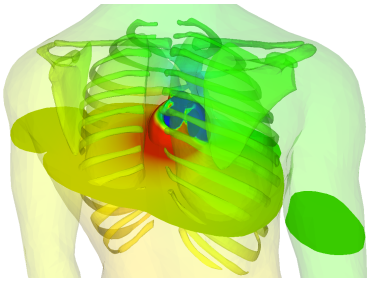

Figure 9: Posterior view and cut plane of the torso and heart potentials at time $t = 10$ ms.

6 Conclusion

We have introduced and analyzed a series of first order semi-implicit time-marching schemes for the cardiac bidomain equations, either isolated or coupled with generalized Laplace equation for the torso. The main feature of the analyzed schemes is that they all allow a fully decoupled computation of the ionic state, the transmembrane potential, the extracellular potential and the torso potential.

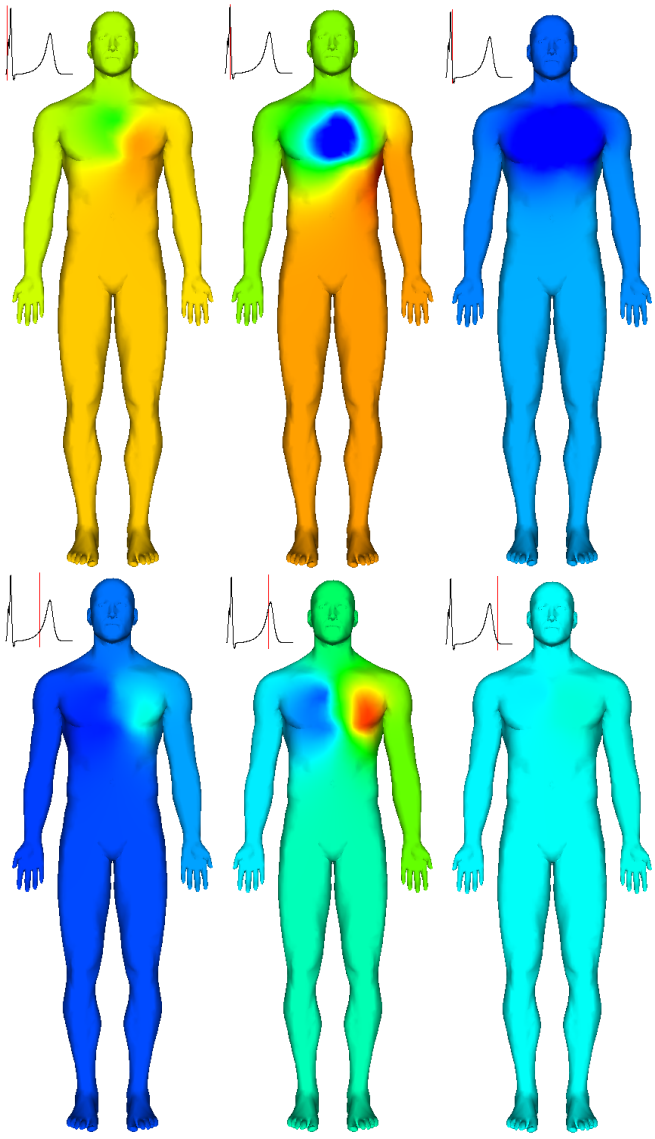

Figure 10: Snapshots of the body surface potentials at times $t = 10$, 32, 40, 200, 250 and 310 ms (from left to right and top to bottom).

For the isolated bidomain model, Theorem 3.2 shows that the Gauss-Seidel and Jacobi splittings do not compromise the stability of the resulting schemes; they simply alter the energy norm. Moreover, the time step restrictions are only dictated by the semi-implicit treatment of then non-linear reaction terms. The numerical results reported in section 5.2 confirmed these theoretical findings.

We extended these time-marching techniques to the numerical simulation of the ECG, by combining the Gauss-Seidel and the Jacobi like bidomain spplitings with an explicit Robin-Robin heart-torso coupling. This specific treatment of the heat-torso coupling is well-suited, particularly, since the time discretization

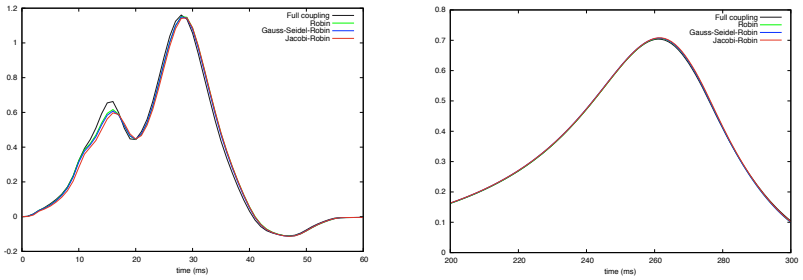

Figure 11: Comparison of the QRS complex (left) and T-wave (right) of the first ECG lead: Full coupling (black), Robin (green), Gauss-Seidel-Robin (blue), Jacobin-Robin (red).

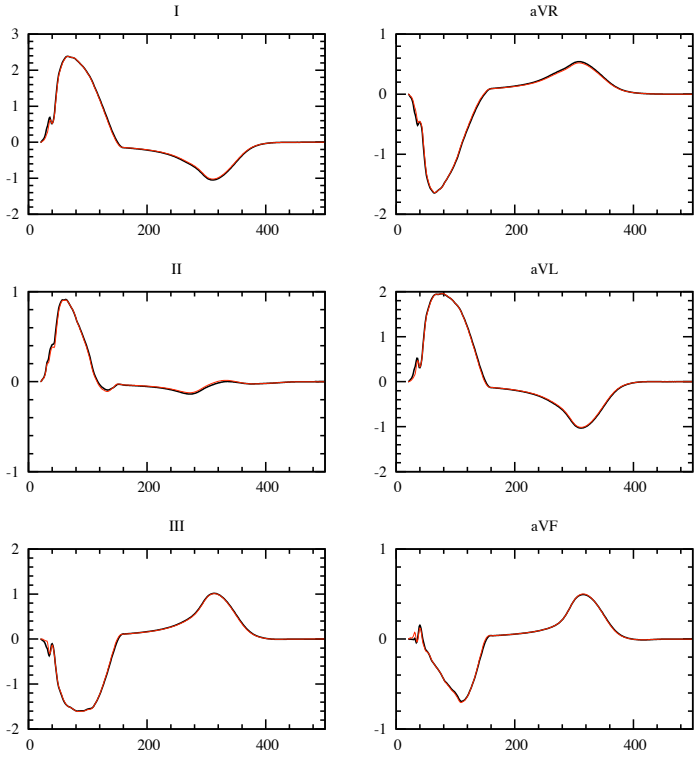

Figure 12: Simulated ECG signals (standard and augmented leads) for a LBBB pathology, obtained using heart-torso full coupling (balck) and the Jacobi-Robin scheme (red).

of the two (quasi-static) elliptic equations does not produce numerical dissipation and, therefore, conventional Dirichlet-Neumann explicit coupling might lead to numerical instability. Theorem 4.4 shows that the proposed splitting schemes are stable under an additional mild CFL like condition $\tau = O(h)$. The numerical study reported in section 5.3, using anatomical heart and torso geometries, demonstrated that the Gauss-Seidel-Robin and the Jacobi-Robin

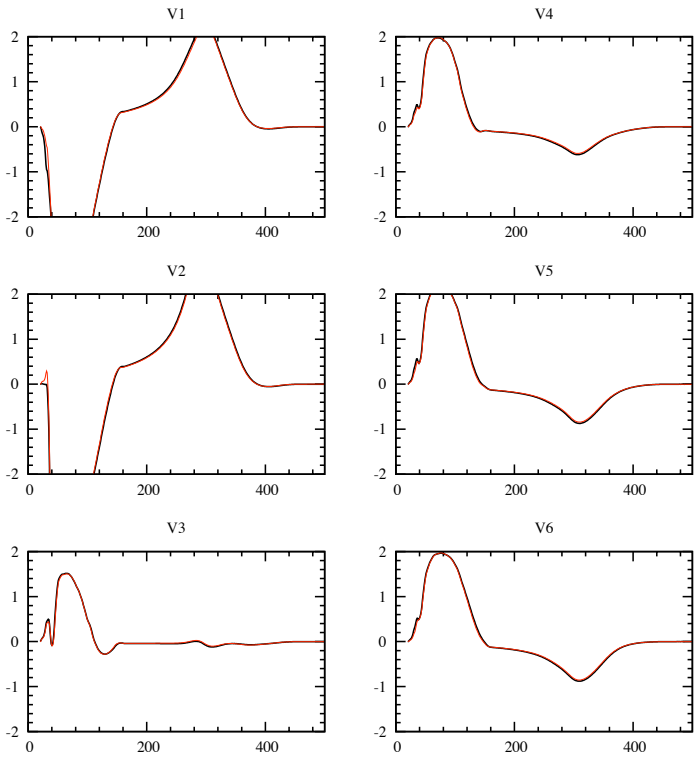

Figure 13: Simulated ECG signals (chest leads) for a LBBB pathology, obtained using heart-torso full coupling (balck) and the Jacobi-Robin scheme (red).

splittings are able to provide accurate 12-lead ECG signals, both for a healthy and a pathological condition. Note that this is a major advantage with respect to the conventional heart-torso uncoupling approximations, which (for a similar computational cost) are known to provide inaccurate ECG signals (see *e.g.* [29, 38, 4]). The robustness of the proposed splitting schemes has been also illustrated with numerical experiments based on different model parameters and heart/torso geometries.

The theoretical and numerical study of this paper is limited to discretizations yielding first order accuracy in time. Some insights into feasible extensions to higher order are commented in Remark 3.4. Although the present stability analysis holds irrespectively of the original time discretization scheme, it does depend on the (first order) extrapolation involved in the splittings. As a result, the generalization of the present analysis to hight order extrapolations seems not straightforward. Further numerical investigations would certainly help to clarify this issue and could be the topic of future work.

Acknowledgements

This work was partially supported by INRIA through its large scope initiative CardioSense3D (`www.inria.fr/CardioSense3D`). We wish to thank Jean-

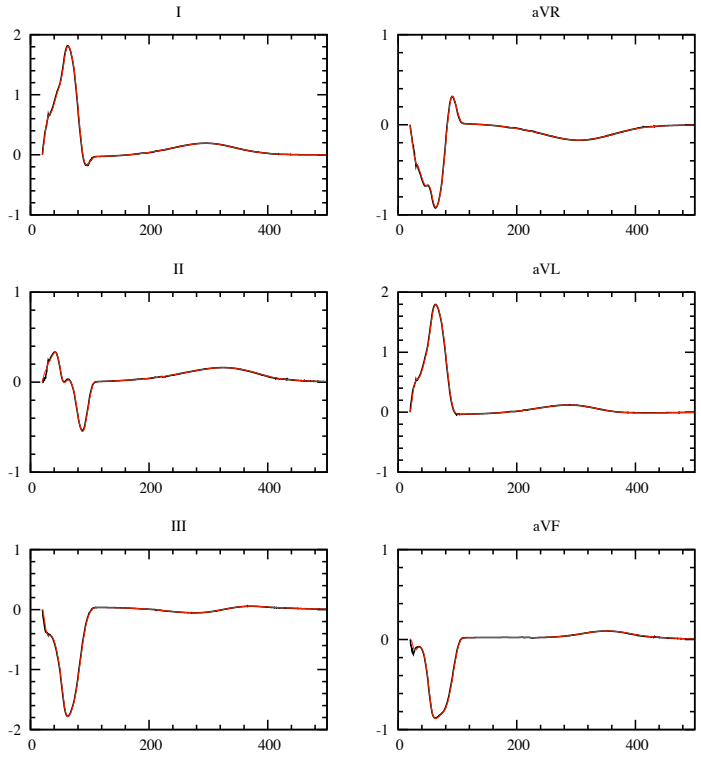

Figure 14: Simulated ECG signals (standard and augmented leads) obtained using heart-torso full coupling (balck) and the Jacobi-Robin scheme (red). Geometry data and model parameters from [4].

Frédéric Gerbeau and Muriel Boulakia for many fruitful discussions on ECG modeling and simulation. We also thank Philippe Moireau and Elsie Phé for their work on the anatomical models and meshes.

References

[1] M. Astorino, F. Chouly, and M.A. Fernández. Robin Based Semi-Implicit Coupling in Fluid-Structure Interaction: Stability Analysis and Numerics. *SIAM J. Sci. Comput.*, 2009. To appear.

[2] T.M. Austin, M.L. Trew, and A.J. Pullan. Solving the cardiac bidomain equations for discontinuous conductivities. *IEEE Trans. Biomed. Eng.*, 53(7):1265–72, 2006.

[3] M. Bendahmane and K.H. Karlsen. Analysis of a class of degenerate reaction-diffusion systems and the bidomain model of cardiac tissue. *Netw. Heterog. Media*, 1(1):185–218, 2006.

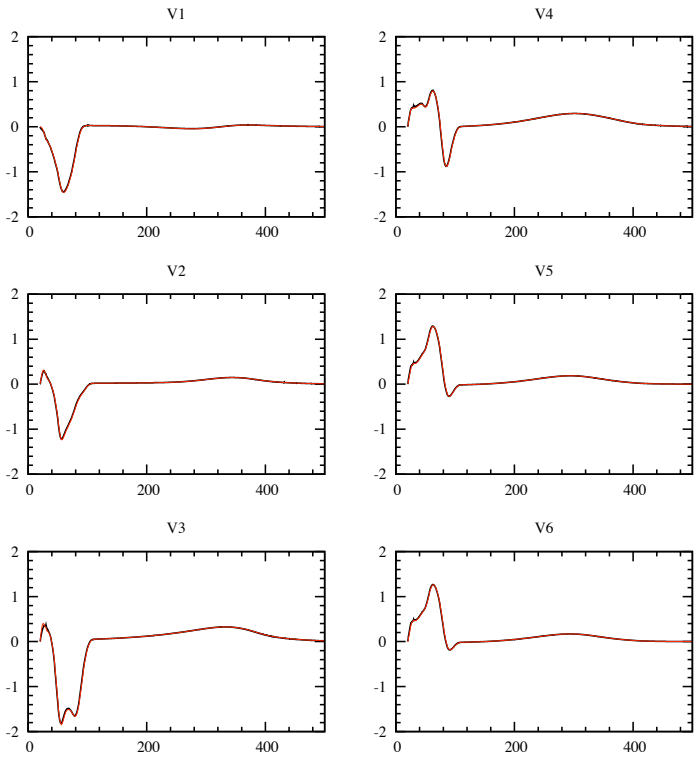

Figure 15: Simulated ECG signals (chest leads) obtained using heart-torso full coupling (balck) and the Jacobi-Robin scheme (red). Geometry data and model parameters from [4].

[4] M. Boulakia, S. Cazeau, M.A. Fernández, J.-F. Gerbeau, and N. Zemzemi. Mathematical Modeling of Electrocardiograms: A Numerical Study. Research Report RR-6977, INRIA, 2009. Submitted.

[5] M. Boulakia, M.A. Fernández, J.-F. Gerbeau, and N. Zemzemi. Towards the numerical simulation of electrocardiograms. In F.B. Sachse and G. Seemann, editors, *Functional Imaging and Modeling of the Heart*, number 4466 in Lecture Notes in Computer Science, pages 240–249. Springer-Verlag, 2007.

[6] M. Boulakia, M.A. Fernández, J.-F. Gerbeau, and N. Zemzemi. A coupled system of PDEs and ODEs arising in electrocardiograms modelling. *Applied Math. Res. Exp.*, 2008(abn002):28, 2008.

[7] Y. Bourgault, Y. Coudière, and C. Pierre. Existence and uniqeness of the solution for the bidomain model used in cardiac electrophysiology. *Nonlinear Anal. Real World Appl.*, 10(1):458–482, 2009.

[8] Y. Bourgault, M. Ethier, and V.G. Le Blanc. Simulation of electrophysiological waves with an unstructured finite element method. *M2AN Math. Model. Numer. Anal.*, 37(4):649–661, 2003.

[9] M. Buist and A. Pullan. Torso coupling techniques for the forward problem of electrocardiography. *Ann. Biomed. Eng.*, 30(10):1299–1312, 2002.

[10] E. Burman and M.A. Fernández. Stabilization of explicit coupling in fluid-structure interaction involving fluid incompressibility. *Comput. Methods Appl. Mech. Engrg.*, 198(5-8):766–784, 2009.

[11] D. Chapelle, M.A. Fernández, J.-F. Gerbeau, P. Moireau, J. Sainte-Maire, and N. Zemzemi. Numerical simulation of the electromechanical activity of the heart. In N. Ayache, H. Delingette, and M. Sermesant, editors, *Functional Imaging and Modeling of the Heart*, volume 5528 of *Lecture Notes in Computer Science*, pages 357–365. Springer-Verlag, 2009.

[12] D. Chapelle, M.A. Fernández, J.-F. Gerbeau, P. Moireau, and N. Zemzemi. A 3D model for the electromechanical activity of the heart. Submitted, 2009.

[13] J. Clements, J. Nenonen, P.K.J. Li, and B.M. Horacek. Activation dynamics in anisotropic cardiac tissue via decoupling. *Annals of Biomedical Engineering*, 32(7):984–990, 2004.

[14] P. Colli Franzone and L.F. Pavarino. A parallel solver for reaction-diffusion systems in computational electrocardiology. *Math. Models Methods Appl. Sci.*, 14(6):883–911, 2004.

[15] P. Colli Franzone, L.F. Pavarino, and B. Taccardi. Simulating patterns of excitation, repolarization and action potential duration with cardiac bidomain and monodomain models. *Math. Biosci.*, 197(1):35–66, 2005.

[16] P. Colli Franzone and G. Savaré. Degenerate evolution systems modeling the cardiac electric field at micro- and macroscopic level. In *Evolution equations, semigroups and functional analysis (Milano, 2000)*, volume 50 of *Progr. Nonlinear Differential Equations Appl.*, pages 49–78. Birkhäuser, Basel, 2002.

[17] I.R. Efimov, R.A. Gray, and B.J. Roth. Virtual electrodes and deexcitation: new insights into fibrillation induction and defibrillation. *J. Cardiovasc. Electrophysiol.*, 11(3):339–353, 2000.

[18] A. Ern and J.-L. Guermond. *Theory and practice of finite elements*, volume 159 of *Applied Mathematical Sciences*. Springer-Verlag, New York, 2004.

[19] M. Ethier and Y. Bourgault. Semi-Implicit Time-Discretization Schemes for the Bidomain Model. *SIAM J. Numer. Anal.*, 46:2443, 2008.

[20] P. Frey. Yams: A fully automatic adaptive isotropic surface remeshing procedure. Technical Report RT-0252, INRIA, Rocquencourt, France, 2001.

[21] P.L. George, F. Hecht, and E. Saltel. Fully automatic mesh generator for 3d domains of any shape. *Impact of Comp. in Sci. ans Eng.*,, 2:187–218, 1990.

[22] R.M. Gulrajani. Models of the electrical activity of the heart and computer simulation of the electrocardiogram. *Crit. Rev. Biomed. Eng.*, 16(1):1–6, 1988.

[23] J.G. Heywood and R. Rannacher. Finite-element approximation of the nonstationary Navier-Stokes problem. IV. Error analysis for second-order time discretization. *SIAM J. Numer. Anal.*, 27(2):353–384, 1990.

[24] N. Hooke, C.S. Henriquez, P. Lanzkron, and D. Rose. Linear algebraic transformations of the bidomain equations: implications for numerical methods. *Math. Biosci.*, 120(2):127–145, 1994.

[25] G. Huiskamp. Simulation of depolarization in a membrane-equations-based model of the anisotropic ventricle. *IEEE Trans. Biomed. Eng.*, 5045(7):847–855, 1998.

[26] J. P. Keener and K. Bogar. A numerical method for the solution of the bidomain equations in cardiac tissue. *Chaos*, 8(1):234–241, 1998.

[27] W. Krassowska and J.C. Neu. Effective boundary conditions for syncitial tissues. *IEEE Trans. Biomed. Eng.*, 41(2):143–150, 1994.

[28] L.J. Leon and B.M. Horácek. Computer model of excitation and recovery in the anisotropic myocardium. I. Rectangular and cubic arrays of excitable elements. *J. Electrocardiol.*, 24(1):1–15, 1991.

[29] G. T. Lines, M. L. Buist, P. Grottum, A. J. Pullan, J. Sundnes, and A. Tveito. Mathematical models and numerical methods for the forward problem in cardiac electrophysiology. *Comput. Visual. Sci.*, 5(4):215–239, 2003.

[30] G.T. Lines, P. Grøttum, and A. Tveito. Modeling the electrical activity of the heart: a bidomain model of the ventricles embedded in a torso. *Comput. Vis. Sci.*, 5(4):195–213, 2003.

[31] S. Linge, J. Sundnes, M. Hanslien, G.T. Lines, and A. Tveito. Numerical solution of the bidomain equations. *Philos. Transact. A. Math. Phys. Eng. Sci.*, 367(1895):1931–1950, 2009.

[32] C.C. Mitchell and D.G. Schaeffer. A two-current model for the dynamics of cardiac membrane. *Bulletin Math. Bio.*, 65:767–793, 2003.

[33] M. Murillo and X.-C. Cai. A fully implicit parallel algorithm for simulating the non-linear electrical activity of the heart. *Numer. Linear Algebra Appl.*, 11(2-3):261–277, 2004.

[34] M. Pennacchio and V. Simoncini. Efficient algebraic solution of reaction-diffusion systems for the cardiac excitation process. *J. Comput. Appl. Math.*, 145(1):49–70, 2002.

[35] M. Potse, B. Dubé, and M. Gulrajani. ECG simulations with realistic human membrane, heart, and torso models. In *Proceedings of the 25th Annual Intemational Conference of the IEEE EMBS*, pages 70–73, 2003.

[36] M. Potse, B. Dube, J. Richer, A. Vinet, and R. M. Gulrajani. A comparison of monodomain and bidomain reaction-diffusion models for action potential propagation in the human heart. *IEEE Trans. Biomed. Eng.*, 53(12):2425–2435, 2006.

[37] M. Potse, B. Dubé, and A. Vinet. Cardiac anisotropy in boundary-element models for the electrocardiogram. *Med. Biol. Eng. Comput.*, 47:719–729, 2009.

[38] A.J. Pullan, M.L. Buist, and L.K. Cheng. *Mathematically modelling the electrical activity of the heart: From cell to body surface and back again.* World Scientific Publishing Co. Pte. Ltd., Hackensack, NJ, 2005.

[39] N. Skouibine, K. Trayanova and P. Moore. A numerically efficient model for simulation of defibrillation in an active bidomain sheet of myocardium. *Math. Biosci.*, 166(1):85–100, 2000.

[40] R.A. Stephenson. On the uniqueness of the square-root of a symmetric, positive-definite tensor. *J. Elasticity*, 10(2):213–214, 1980.

[41] H.J. Stetter. The defect correction principle and discretization methods. *Numer. Math.*, 29:425–443, 1978.

[42] J. Sundnes, G.T. Lines, X. Cai, B.F. Nielsen, K.-A. Mardal, and A. Tveito. *Computing the electrical activity in the heart.* Springer-Verlag, 2006.

[43] J. Sundnes, G.T. Lines, and A. Tveito. Efficient solution of ordinary differential equations modeling electrical activity in cardiac cells. *Math. Biosci.*, 172(2):55–72, 2001.

[44] J. Sundnes, G.T. Lines, and A. Tveito. An operator splitting method for solving the bidomain equations coupled to a volume conductor model for the torso. *Math. Biosci.*, 194(2):233–248, 2005.

[45] V. Thomée. *Galerkin finite element methods for parabolic problems*, volume 25 of *Springer Series in Computational Mathematics*. Springer-Verlag, Berlin, second edition, 2006.

[46] L. Tung. *A bi-domain model for describing ischemic myocardial D–C potentials.* PhD thesis, MIT, 1978.

[47] M. Veneroni. Reaction-diffusion systems for the macroscopic bidomain model of the cardiac electric field. *Nonlinear Anal. Real World Appl.*, 10(2):849–868, 2009.

[48] E.J. Vigmond, R. Weber dos Santos, A.J. Prassl, M Deo, and G. Plank. Solvers for the cardiac bidomain equations. *Progr. Biophys. Molec. Biol.*, 96(1–3):3–18, 2008.

Contents

Unité de recherche INRIA Rocquencourt
Domaine de Voluceau - Rocquencourt - BP 105 - 78153 Le Chesnay Cedex (France)

Unité de recherche INRIA Futurs : Parc Club Orsay Université - ZAC des Vignes
4, rue Jacques Monod - 91893 ORSAY Cedex (France)
Unité de recherche INRIA Lorraine : LORIA, Technopôle de Nancy-Brabois - Campus scientifique
615, rue du Jardin Botanique - BP 101 - 54602 Villers-lès-Nancy Cedex (France)
Unité de recherche INRIA Rennes : IRISA, Campus universitaire de Beaulieu - 35042 Rennes Cedex (France)
Unité de recherche INRIA Rhône-Alpes : 655, avenue de l'Europe - 38334 Montbonnot Saint-Ismier (France)
Unité de recherche INRIA Sophia Antipolis : 2004, route des Lucioles - BP 93 - 06902 Sophia Antipolis Cedex (France)

Éditeur
INRIA - Domaine de Voluceau - Rocquencourt, BP 105 - 78153 Le Chesnay Cedex (France)
http://www.inria.fr
ISSN 0249-6399